MRes Literature Review

Title: Metal Doped Porous Carbons for Use in Energy Applications: A Review

Student's name: Elliot Findlay

Student ID Number: 14274306

Supervisor: Robert Mokaya

Assessor: -

Acknowledgements

Abstract

With a rapidly growing world population and rising global temperatures, a need for a green energy store to replace fossil fuels is more necessary than ever. Many methods and materials have been put forward as candidates, such as Li-ion batteries, supercapacitors, solar-powered cells, and hydrogen fuel cells. However, many of these methods are not fully optimised and cannot realistically compete with fossil fuels. Supercapacitor electrodes made from activated carbon or graphene often lack a large enough capacitance to compete with Li-ion batteries as an efficient energy store, and transition metal oxides have been known to increase capacitance of various materials. This review compares and contrasts the capacitive abilities of various transition metal oxide-doped activated carbon and graphene composites, for use as supercapacitor electrodes, in comparison to their pristine counterparts. Another major problem with new energy stores is the efficient and safe storage of molecular hydrogen, for a potential hydrogen economy. This review explores the use of various metals as dopants for increasing the hydrogen uptake capacities of activated carbons, as well as other carbon based hydrogen stores.

Contents

2. Project Aims

3. Metal Doped Carbons in Energy Applications

3.1 Electrochemical Applications

3.1.1 M and MO/Activated Carbon Supercapacitor Electrodes

3.1.2 M and MO/Graphene Supercapacitor Electrodes

3.2 Hydrogen Storage

3.2.1 M/Activated Carbon H_2 Stores

3.2.2 M/Graphene and Graphene Oxide H_2 Stores

3.2.3 M/Fullerene H_2 Stores

4. Conclusions

5. References

1. Introduction

1.1 The Climate Crisis and Sustainable Energy

Global warming is the name given to the increase in rising average global temperatures that has been observed since the mid-1900s. Global warming leads to changes in local climates, increases of extreme weather, and the melting of the polar ice caps, which cause rising sea levels. Data from NASA shows that human drivers are the leading cause of global warming, with the largest influence coming from greenhouse gas emissions.[1]

Greenhouse gases (GHGs) are gases that are present in the atmosphere and that absorb and emit infrared energy. The main GHGs in the Earth's atmosphere are carbon dioxide (CO_2), methane, ozone, water vapour and nitrous oxide. There is a positive correlation between the concentration of CO_2 in the atmosphere, and the temperature of the Earth's surface. CO_2 is the by-product of all fossil fuel consumption processes, and in 2016, 54.1% of the UK's energy came from fossil fuels (42% natural gas, 9% coal and 3.1% other). The Intergovernmental Panel on Climate Change (IPCC) concluded that a 1.5°C increase in Earth's surface level, compared to levels in the pre-industrial age, would pose a catastrophic risk to human and wildlife ecosystems.[2] Nearly every nation of the world is a member of the United Nations Framework Convention on Climate Change (UNFCCC), whose role is to mitigate the rate of global warming by primarily switching to "clean" and renewable technologies such as wind and solar power, hydrogen and battery powered vehicles, nuclear energy, etc.

Not only do fossil fuels produce greenhouse gases that pollute the atmosphere, but they also have economic and political drawbacks. Crude oil prices can fluctuate wildly and rapidly depending on policies, the market and the news cycle. For example, in November 1985 the price per barrel was $70.72, but in March 1986 it dropped to $24.81, only to rise to $37.56 that August. Furthermore, the reserves of crude oil and natural gas in the world are unevenly distributed.[3] In 2015 the US imported 19% of all its oil from the Middle East.[4][5] This uneven distribution can lead to conflict and political instability in these regions. Moreover, fossil fuels are non-renewable and so there is a finite amount of crude oil and natural gas in the world. It is estimated by the IPCC that fossil fuel reserves will run out by as soon as 2060 if our society burns them at the same rate as it does now.

This problem now leaves us with an important question: what will replace fossil fuels? For the issue of vehicles, opinion is somewhat divided between battery powered cars and hydrogen powered cars. Both options have their advantages and disadvantages, and neither are fully optimised enough to compete with fossil fuels. Various forms of metal (M) and metal oxide (MO) doped porous carbons may possess the solution for optimisation of both these renewable energies. In this review, it will be

discussed how introducing M/MO to a porous material can improve its electrochemical properties for use in supercapacitors, and how they can improve hydrogen gas uptake for use in a potential "hydrogen economy."

1.2 Supercapacitors and Li-Ion Batteries as Green Energy Sources

1.2.1 Lithium-Ion Batteries

Lithium-Ion, Li-ion Batteries or LIBs are the world's most commonly used battery for electric vehicles and portable electronics. Electric vehicles are a popular choice for green transport due to their carbon neutral functionality, but they are not without their flaws. During the discharge cycle, Li ions move from anode to the cathode through the electrolyte, which can be solid or liquid, and the reverse during the charging cycle. LIBs have a high energy density and a low self-discharge, making them excellent for powering electronics that need a long battery life. However, due to their low self-discharge they are not good at bursts of power. Furthermore, LIBs with liquid electrolytes possess significant safety hazards due to the flammability of the electrolyte. If the cell is pierced, Li-ion batteries have been known to violently catch fire and sometimes explode. This is one of the biggest advantages of solid electrolytes, as they are not pyrophoric and therefore pose no safety threat when compromised.

The positive electrode is always a lithium-containing compound such as lithium cobalt oxide ($LiCoO_2$), a particular LIB designed by John Goodenough in 1980 and commercialised by Sony in 1991.[6] The materials used for the negative electrode differ substantially. Traditionally, lithium intercalated graphite is used as the material for the negative electrode, however, research in recent years has attempted to replace graphite with silicon or activated carbons. Activated carbons are already used as a solid electrolyte material in LIBs due to their porosity allowing a shortened transport length for the Li ions. They are also an excellent material for Li-Ion battery anodes and have been proven to have a higher capacity than graphite anodes.[7]

1.2.2 Supercapacitors

Common industrial supercapacitors have several similarities with batteries but have many different strengths and weaknesses. Compared to a battery of the same size, supercapacitors have a quicker charge/discharge rate and a longer cycle life due to the higher power density. They also have a longer shelf life as there is no chemical reaction occurring at the electrodes, as well as a wider range of operating temperatures.[8][9] However, they also have a lower energy density, and the self-discharge is much higher. Hence supercapacitors are used in electronics where short bursts of power are

needed. For example, in a camera flash, for an emergency shutdown in a computer, or to support peak demand times in the national grid. They are also useful in applications with frequent charge and discharge cycles, such as in regenerative breaking in electric cars.

In a conventional parallel plate capacitor, charges are separated to induce voltage by charging opposite plates with a non-conductive material (dielectric) in between. Capacitance is given by the equation:

$$C = \frac{\varepsilon_0 \varepsilon_r A}{d}$$ [Equation 1]

$\varepsilon_0 =$ Permittivity of Free Space

$\varepsilon_r =$ Dielectric Constant

The higher the capacitance, the better the device is at storing charge. Therefore, a larger plate surface area (A) and a smaller charge separation distance (d) owe to a higher value of capacitance.

There are two types of electrochemical supercapacitors: Electric double-layer capacitors (EDLCs) and pseudocapacitors.[10] In a pseudocapacitor, energy is stored through fast and reversible faradaic charge transfer between active species on the electrode and the electrolyte. In an EDLC the dielectric of a conventional capacitor is replaced with an electrolyte and electrodes are made of extremely pure activated carbons and so charge occurs by the formation of electrical double layers. When a current is induced, ions in the electrolyte move to oppositely charged electrodes. The first layer of the double layer is a dense layer of ions attracted to an oppositely charged electrode and is called the Diffuse, layer, or Helmholtz layer. These ions do not touch the electrode as they are separated by a specifically adsorbed layer of solvent molecules. This creates the charge separation, d, which naturally will be much smaller than that of a conventional capacitor, owing to a supercapacitor's higher capacitance. The second layer is called the diffuse layer and is made up of ions diffusing to the Helmholtz layer. Therefore, a supercapacitor can be represented by two capacitors separated by a resistor, resistance arises from diffusion of ions and hence energy loss. The greater capacitance is why supercapacitors are thought of as an intermediate energy source between capacitors and batteries.[11]
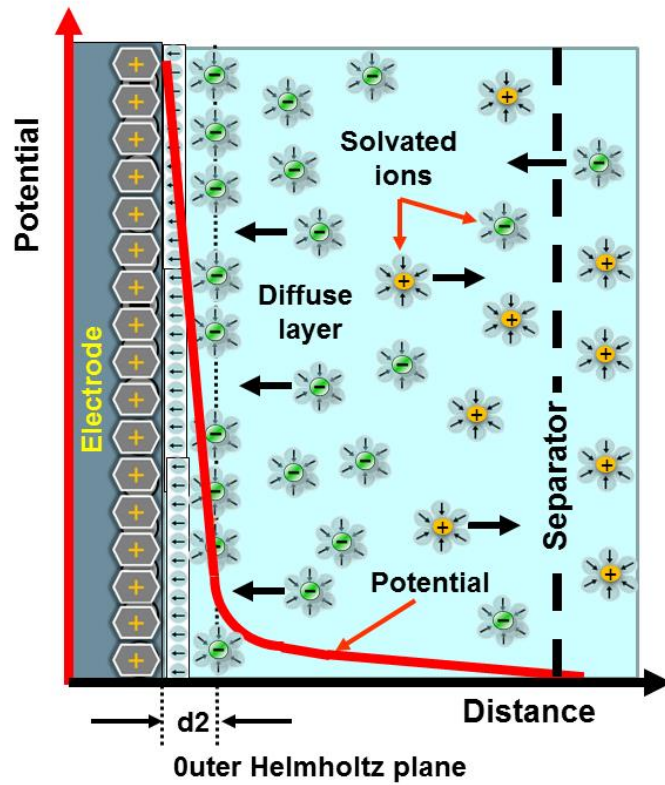
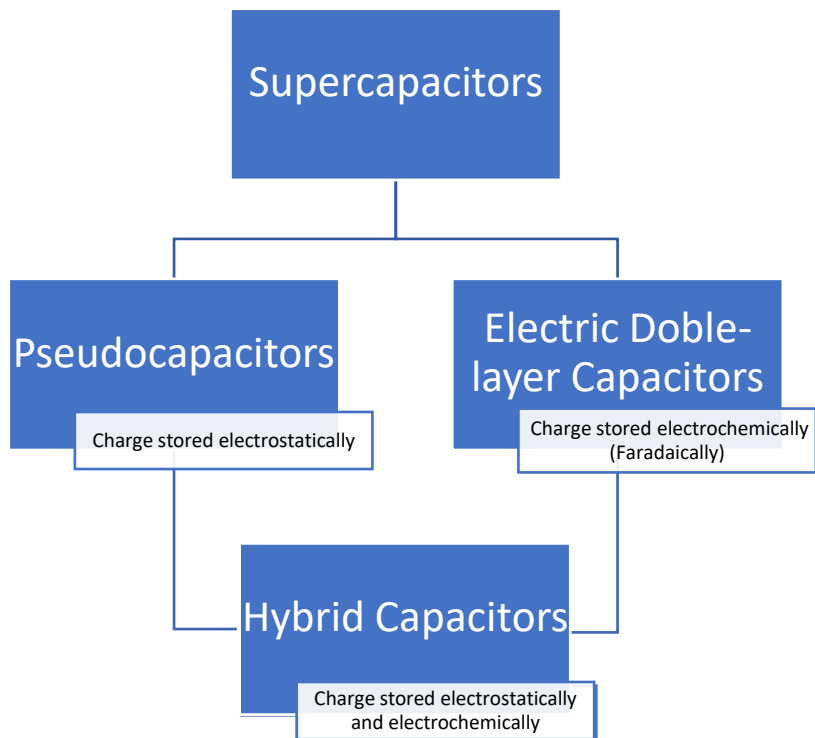**Fig 1. Double layer capacitance**

Fig 2. Different types of capacitors and how they store charge.

Because supercapacitors still have low energy density of 5-10 Wh/kg (compared to 120-170 Wh/kg from a Li-ion battery), capacitance must be increased to make them competitive with modern Li-ion batteries.[11] EDLCs have excellent power densities and life cycles, but also have low energy densities, whereas, pseudocapacitors have been shown to have higher capacitance than EDLCs, but also have poor cycle life.[12] Therefore, a relatively new type of supercapacitor called a hybrid capacitor, which takes advantage of both mechanisms, has been explored. To further increase capacitance, the carbon electrodes can be doped with metals and metal oxides to make metal-carbon composites. This paper will review which metals are most effective at doing this job. As shown in equation 1, using a high surface area material for the electrodes gives a higher capacitance. Because of this, graphene is a promising material for supercapacitors.

1.3 Graphene as a Supercapacitor Electrode Material

Currently, the vast majority of electric double-layer (EDL) supercapacitors use activated carbon as the material for the electrode, due to its high surface area, which as explained by equation 1, results in a larger capacitance.[13] Despite this, only 10-20 % of the theoretical capacitance is observed from an activated carbon based EDL supercapacitor.[14][15] This is due to the presence of micropores which are too small for the electrolyte to access the internal surface. Furthermore, some pores which are large enough for the electrolyte are not large enough for the formation of a double-layer. Recent studies show that carbon nanotubes (CNTs) exhibit poor capacitance when used in in EDLCs.[15]

Graphene, a two-dimensional, single sheet of graphite, has shown exceptional capacitance, as well as high tensile strength, electrical and thermal conductivity, and specific surface area.[16-19] The surface area of pristine graphene can be up to 2675 m^2g^{-1}, which is on par with some activated carbons, and its intrinsic capacitance is 21 μFcm^{-2}, which is the highest recorded capacitance of any pure carbon-based EDLC.[20][21] It has also been demonstrated that using graphene electrodes with an ionic liquid electrolyte can produce EDL supercapacitors with unprecedented energy densities of up to 90 Wh/kg at room temperature, which is almost competitive with Li-ion batteries.[13] This is achieved by using curved, mesoporous graphene in place of pristine graphene, which allows the large ions in the electrolyte to access the full surface area, as well as prevent stacking of the graphene sheets.

1.4 The Hydrogen Economy

Other than electric vehicles, one of the biggest contenders for the replacement of fossil fuels is hydrogen power. The hydrogen economy is a hypothetical future in which the worlds primary energy store is molecular hydrogen (H_2). The term was first used at the General Motors technical centre by John Bockris in 1970, however, the concept had existed much earlier. The system includes all sectors of modern society from vehicles to power plants to mobile phones. As explained earlier there are many extreme disadvantages to using fossil fuels as a primary fuel source and so an alternative energy is required to sustain the growing population. Many scientists believe battery power can be the answer, but Li-ion batteries share some of the same geopolitical drawbacks of fossil fuels. Cobalt is a major component of modern Li-ion batteries and it is estimated that 25% of the worlds cobalt supply comes from the Democratic Republic of Congo (DRC), a country that is still recovering from several conflicts in the 1990s and to this day is considered a politically unstable country. Another one of the world's biggest exporters of cobalt is Russia, another country where tensions between it and the west could rise at any moment.

Hydrogen, however, is abundant across the globe. While the primary means of hydrogen production today is steam-reformation of natural gas, scientists are working on making water electrolysis (a carbon neutral means of obtaining hydrogen) more efficient for the future of hydrogen energy. Hydrogen is not found in its elemental form, it must be obtained from fossil fuels or water, hence energy is needed to obtain it. Therefore, hydrogen is referred to as an energy store rather than an energy source. Hydrogen is also safer than petrol and diesel powered vehicles. If a petrol tank were to leak, the liquid would spill over the ground, and in the event of a fire the surrounding area would be engulfed in flames. On the other hand, if a hydrogen fuel tank leaked the gas would disperse into the air.

By weight, hydrogen has three times as much energy as petrol per kilogram. But if the energy density is compared, hydrogen has four times less energy than petrol per litre (see table 1). Therefore, we must store hydrogen as efficiently as possible in order to increase the energy density, this is where hydrogen storage materials, namely activated carbons, play a large role.

	Petrol	Hydrogen
Energy per Kilogram	40 MJ kg^{-1}	120 MJ kg^{-1}
Energy Density	32 MJ L^{-1}	8 MJ L^{-1}

Table 1. Comparison of the energy density and specific energies of petrol and hydrogen.

1.5 Hydrogen Storage Techniques

As discussed in **1.4**, the low density of hydrogen gas makes it extremely difficult to store useful quantities at room temperature. Therefore, various materials are used to increase the amount of hydrogen that can be stored in a fixed volume as near to room temperature and pressure as possible. The US Department of Energy (DoE) continuously sets requirements for hydrogen storage materials for hydrogen powered vehicles to reach by 2025 (see table 2). It stated the material must be able to carry enough hydrogen for at a minimum 300 miles. It also stated that the material must be flexible, compact, safe and light. Methods and materials for hydrogen storage can be subdivided into 3 techniques. The first being physically compacting the hydrogen gas either by compression or using liquid H_2. These techniques, however, are extremely inefficient and energy consuming, so lots of research has been put into looking at materials that can store hydrogen either through chemisorption or physisorption. This leads us to the second technique which is chemical storage, which refers to hydrogen being released through chemical reaction. The main chemicals used for this method are metal hydrides, however, using these come with some serious safety hazards due to the reactive nature of hydrides. The final method for hydrogen storage is to use porous materials such as activated carbons, metal organic frameworks (MOFs) or porous polymers.

STORAGE PARAMETER	UNITS	2020	2025	ULTIMATE
System Gravimetric Capacity				
Usable, specific-energy from H_2 (net useful energy/max system mass) [b]	kWh/kg (kg H_2/kg system)	1.5 (0.045)	1.8 (0.055)	2.2 (0.065)
System Volumetric Capacity				
Usable energy density from H_2 (net useful energy/max system volume) [b]	kWh/L (kg H_2/L system)	1.0 (0.030)	1.3 (0.040)	1.7 (0.050)
Storage System Cost				
Storage system cost	$/kWh net ($/kg H_2)	10 (333)	9 (300)	8 (266)
Fuel cost [c]	$/gge at pump	4	4	4
Durability/Operability				
Operating ambient temperature [d]	°C	-40/60 (sun)	-40/60 (sun)	-40/60 (sun)
Min/max delivery temperature	°C	-40/85	-40/85	-40/85
Operational cycle life (1/4 tank to full)	cycles	1,500	1,500	1,500
Min delivery pressure from storage system	bar (abs)	5	5	5
Max delivery pressure from storage system	bar (abs)	12	12	12
Onboard efficiency [e]	%	90	90	90
"Well" to power plant efficiency [f]	%	60	60	60
Charging/Discharging Rates				
System fill time [g]	min	3–5	3–5	3–5
Minimum full flow rate (e.g., 1.6 g/s target for 80 kW rated fuel cell power)	(g/s)/kW	0.02	0.02	0.02
Average flow rate	(g/s)/kW	0.004	0.004	0.004
Start time to full flow (20°C)	s	5	5	5
Start time to full flow (-20°C)	s	15	15	15
Transient response at operating temperature 10%–90% and 90%–0% (based on full flow rate)	s	0.75	0.75	0.75
Fuel Quality				
Fuel quality (H_2 from storage) [h]	% H_2	Meet or exceed SAE J2719		
Dormancy [i]				

Table 2. 2025 targets for light-duty hydrogen powered vehicles. [22]

1.5.1 Physical Storage

Compressed H_2

Most modern H_2 compressors fit into 2 types: Positive displacement compressors or centrifugal compressors. Positive displacement compressors have a piston that is moved back and forth by a motor which reduces the volume that the hydrogen occupies, hence compressing it. Reciprocating compressors are a type of positive displacement compressor and are the most common used compressor for transport due to the high compression ratio of 1.2 to 4.0. Alternatively, centrifugal compressors contain a turbine that is rotated at high speed and are used in pipelines due to the medium compression ratios.

Other types of compressor also exist such as ionic compressors that use ionic liquids instead of a piston which reduces the number of components, and hence the chance of system failure. These compressors are ideal for H_2 fuel stations. Compressors are often combined with other storage types such as metal hydrides to further reduce the volume the H_2 occupies. However, the biggest drawback

of compressors is that the high-pressure tanks are heavy, large and do not store enough H_2 on their own. Therefore, they can only really be used for stationary purposes.

Liquid H_2

Storing H_2 as a liquid is preferable as it has a higher energy density than gas, therefore smaller tanks can be used for the same amount of fuel. However, cryogenic temperatures are needed to keep it as a liquid as the boiling point of hydrogen is -253 °C. This requires a lot of energy and an efficiency loss of roughly 40%.[23] Furthermore, 3-4% of the liquid H_2 is lost per day to the surface layer boiling off. Liquifying H_2 can be combined with compression in a technique called cryo-compression, which limits the amount of H_2 that is lost to boiling off. This technique still uses vast amounts of energy and is still very expensive. It is clear that compressing or liquifying H_2 is not efficient enough for a hydrogen economy, and so other storage techniques must be used, especially for mobile applications.

1.5.2 Chemical Storage

Metal Hydrides

Commonly used hydrides used for H_2 uptake are LiH, MgH_2, $NaAlH_4$ and palladium hydride. Metal powders are deposited in compressed tanks and the hydrogen chemisorbs onto the metal to form metal hydrides. These tanks can store up to 740 L of H_2 gas, however, these are not without their disadvantages. The largest problem with metal hydride storage is the reversibility of the adsorption process. Like many hydrogen storage materials, high temperatures are needed to dissociate the H_2 and so the main area of research is lowering these temperatures. One way of doing this with metal hydrides is by adding activating or destabilising agents, although this makes the synthesis overly complex. Due to the requirements imposed by the DoE, heavier metals, that can take more hydrogen atoms, can only be used as low-abundance additives.[24] In a study by J. Vajo *et al* $LiBH_2$ and Mg_2 were mixed together which showed significant decrease in the dissociation enthalpy of H_2, with a maximum H_2 uptake of 11.4 wt %.[25] This was achieved by the formation of MgB_2 which destabilizes $LiBH_4$ and stabilizes the dehydrogenated state. Another issue with metal hydride storage is that metal hydrides are reactive with oxygen-containing organic compounds, hence great care must be taken when researching new and more optimised storage systems.

Amines

Using a catalytic reformer, hydrogen can be obtained from ammonia gas. The boiling point of ammonia is -33.3 °C therefore is takes very little energy to liquify ammonia and hence increase the hydrogen storage ability. Furthermore, if combined with water, it can be stored at room temperature and

pressure. The only by-product of the reaction is dinitrogen gas, so this method is both carbon neutral and toxic waste-free. However, after reformation, small amounts of ammonia will remain. Ammonia gas is toxic and has a potent odour. Therefore, a way of separating ammonia from H_2 is necessary.

Hydrazine is a compound previously used as a monopropellant aboard space craft. When passed over an iridium catalyst it decomposes into ammonia, nitrogen and hydrogen gas. As a product of decomposition is hydrogen, hydrazine can be used as a chemical hydrogen store. While hydrazine is efficient at storing H_2 and thermodynamically favours the formation of H_2, it poses serious fire risks due to its energetically reactive nature and is also extremely toxic.

Organic Compounds

Unsaturated organic compounds such as cycloalkanes and N-heterocycles can be hydrogenated to store hydrogen and dehydrogenated when the fuel is needed. When used for H_2 storage these compounds are called liquid organic hydrogen carriers (LOHCs). An example of an LOHC is N-ethylcarbazole, which can be hydrogenated 6 times, hence can store 12 hydrogen atoms. Similar to metal hydrides, high temperatures are needed to dehydrogenate LOHCs as the reverse reaction is highly endothermic. Therefore, a metal catalyst is needed to lower the enthalpy of the reaction. Metals under study for dehydrogenation are molybdenum and platinum, but these metals are expensive and long-term stability is an issue.[26]

1.5.3 Porous Materials

Activated Carbons

Activated carbons are carbon-based molecules and structures that have gone through an activation process which greatly increases the surface area by creating <9 Å micropores throughout the carbon network. These two factors allow for the highest storage levels of hydrogen. However, the interaction between H_2 molecules and the surface of the pores is weak at ambient temperature, and so research is based around functionalisation of the pores to create stronger interactions with hydrogen. Other than the high surface area, the other benefit of activated carbons is that they can be derived from waste materials such as discarded plastic and cigarette butts. Activated carbons will be discussed in greater detail in **1.6**.

Metal Organic Frameworks

A metal organic framework or (MOF) is a coordination network of organic ligands. A coordination network is a coordination compound extending through repeating coordination entities.[27] They can be thought of as a repeating structure of metal ions connected by bridging ligands. Between these

ligands are potential voids, of which the size can be controlled very easily by selecting the metals and ligands that create the structure. These voids are used to store hydrogen, with the highest theoretical usable gravimetric (UG) capacity belonging to MOF-399: 19.3 wt%.[28] This figure is not taking into account usable volumetric (UV) capacity. MOFs are often thermodynamically unstable and are very sensitive to moisture. Structural defects are often present in MOFs as well.

Carbon Allotropes

Graphene and fullerenes can be used as a hydrogen store as the H_2 molecules associate onto the carbon atoms to create graphane $(CH)_n$ and theoretically $C_{60}H_{60}$. However, the dissociation temperatures for these additions is 450 °C and 600 °C respectively,[29] and pure graphene alone does not store enough hydrogen to fulfil the 6 wt% target set by the DoE.

Carbon nanotubes are used differently to graphene and fullerenes. They are doped with metal hydrides which chemically store hydrogen, and the nanotube is used as a means of a fast diffusion channel in an effort to decrease the dissociation temperature of metal hydrides. Carbon allotropes will be discussed further in **1.7**.

Zeolites

Zeolites are a group of porous materials made from silica and alumina and can be found naturally or synthesized in a lab. The general structure of a zeolite is $M_{x/n}[(AlO_2)_x(SiO_2)_y].mH_2O$, where M is a counter ion to balance the overall negative charge of the framework. The structure is made up of corner-sharing $[AlO_2]^{5-}$ and $[SiO_2]^{4-}$ tetrahedra, which create cavities in which hydrogen can be stored. Unlike MOFs, zeolites have excellent thermal and chemical stability. However, zeolites are much less "customisable" and so, they cannot be optimized as easily as MOFs or carbon materials. Because of this, zeolites have a low hydrogen uptake in comparison, with the highest recorded belong to zeolite CaX at 2.19 wt%.[30] Zeolites can be used as a template for porous carbons, which can then be later optimized by heteroatom doping to improve upon the hydrogen uptake. The benefit of using this method for generating porous carbons is that the structure is highly ordered, something that is not possible with activated carbons.[31]

Porous Polymers

Polymers with intrinsic porosity (PIMs) are polymers that are specifically designed to have pores of less than 2 nm in width. This porosity is achieved by creating a polymer with a rigid, kinked backbone, which limits rotational freedom and hence efficient packing. An example of one of these materials is PIM-1 (see fig 3), which has been shown to have one of the largest surface areas of any PIM.
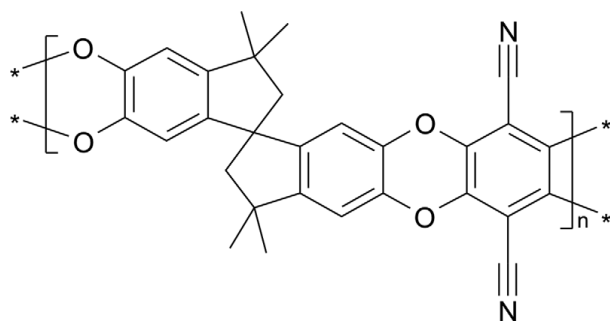
Fig 3. Structure of PIM-1.

A large advantage of using PIMs as hydrogen stores is that they are often soluble and easy to handle. Moreover, the starting materials needed to sythesize these structures are cheap and readily accesible. One major disadvantage of PIMs is that their surface area is much smaller in comparison to activated carbons; 800 $m^2\,g^{-1}$ versus 4000 $m^2\,g^{-1}$ respectively. Therefore, PIMs as they are currently cannot ever store as much hydrogen as activated carbons or MOFs.

Glass Microspheres

Hollow glass microspheres (HGMs) are used to store hydrogen at room temperature and pressure which is extracted through the porous walls at high temperature and pressure. The biggest benefits of HGMs are that they store hydrogen at room temperature, although high temperature and pressure is needed to initially force the hydrogen into the HGMs, and that they are easy to handle, cheap and recyclable.[32] Due to the insulating nature of glass, rapid hydrogen diffusion is not possible with HGMs without a transition metal dopant, in order to improve the conductive properties of the HGMs.

1.6 Activated Carbons for Use in Supercapacitors and Hydrogen Stores

Activated carbons are carbonaceous materials that have been either physically or chemically activated to give them a high degree of porosity and larger surface area. It is due to these two factors that activated carbons are key materials in the production of supercapacitor electrodes and hydrogen storage materials, and hence why they will be the focus of this review. Not only are activated carbons used in green energy solutions, but are also used in almost every purification system today such as water and air filters, as well as respiratory masks for airborne diseases. For gas adsorption uses, activated carbons are usually microporous or mesoporous, where microporous is having pores of less than 2 nm wide, and mesoporous is having pores between 2 and 50 nm.[33] Precursors for activated carbons can be realistically anything that is organic; for example, corn husks, wood (e.g. Eucalyptus),

peat, cigarette butts, and polymers such as polypyrrole and polyethylene. These starting materials are called feedstocks, and the organic feedstocks are called biomass.

1.6.1 Activation

There are two distinct ways of activating carbonaceous materials: Physical or chemical activation. Physical activation is a two-step process and begins with heating the starting material to temperatures above 400 °C in an inert atmosphere. At these temperatures pyrolysis occurs, which is the thermal degradation of the feedstock to produce char. This first step is called carbonization as what is left after pyrolysis is mainly carbon. The carbonized material is then heated up again above 350 °C in the presence of an oxidising gas, which is usually oxygen, CO_2 or steam. The activating gas physically opens pores by passing through the material, and also reacts with volatile matter that remains after pyrolysis, leaving only the most stable regions of the carbonized material. The nature of the activated carbons made from this method are dependent on the feedstock, activating gas and temperature of activation. Physical activation is less desired as it requires higher temperatures and more steps. Furthermore, physically activated carbons tend to produce lower yields due to the destructive nature of the synthesis.

Chemical activation is much more frequently used as the method of choice when it comes to research purposes, especially for gas adsorption. This is because of the higher surface area produced ($3600 \ m^2g^{-1}$) and also because the pore size distribution (PSD) can be easily altered by changing the temperature of activation and/or the ratio of activating agent to precursor. A study by S. Ghosh *et al* showed that the mass ratio of KOH : Precursor for efficient storage of CO_2 is 3:1.[34] Carbon precursors are activated chemically by mixing with activating agents such as potassium hydroxide (KOH), sodium hydroxide (NaOH) or phosphoric acid (H_3PO_4). This reaction is carried out at high temperature (700-900 °C) inside a horizontal tube furnace under the flow of an inert gas, usually nitrogen. KOH is by far the most used activating agent due to its ability to produce carbons with exceptionally high surface area. KOH reacts with carbon in the starting material to produce potassium metal, hydrogen gas and potassium carbonate, seen in the reaction scheme below.

$$6 \ KOH + 2 \ C \longleftrightarrow 2 \ K + 3 \ H_2 + 2 \ K_2CO_3$$

$$K_2CO_3 \rightarrow K_2O + CO_2$$

Potassium carbonate then thermally decomposes into K_2O and CO_2 at temperatures above 700 °C. It is this production of CO_2 that creates pores within the structure. After pyrolysis, the products must be washed in hydrochloric acid to reveal the pores. It has been shown that at higher ratios of

KOH:Precursor and temperature, pore volume will increase, however, this is paired by an increase in PSD (see fig 4 and 5). Therefore, for efficient gas storage, higher concentration of activating agent is not necessarily better.
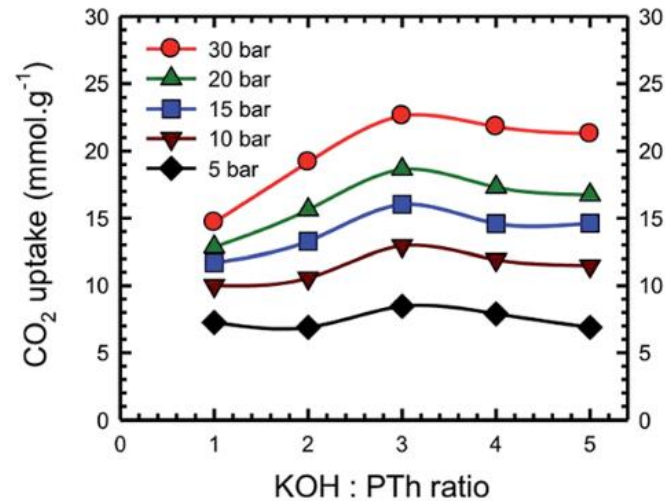

Fig 4. CO_2 uptake peaks at ratio of 3:1 (KOK : PTh, where PTh is Polythiophene)
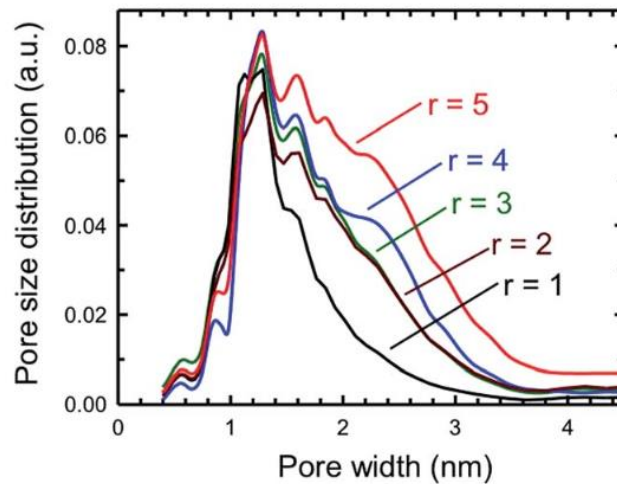

Fig 5. Increasing PSD with increasing ratio of KOH : PTh.

1.6.2 Hydrothermal Carbonisation

As stated in **1.6** and 1.5.3, activated carbons can be derived from biomass, such as rice husks, wood dust and peat. These materials cannot be activated directly, and similar to physical activation, the materials must be pyrolyzed first in a process called hydrothermal carbonisation. The process involves heating polysaccharide (usually cellulose) biomass in water, inside a pressurised cylinder. The final product of hydrothermal carbonisation is a substance called "hydrochar," which has been shown to be made up of hydrophilic microspheres. Polysaccharides decompose into oligomer, water soluble

fragments above 200 °C, and then further into glucose monomers.[35] These products of decomposition then undergo a series of reactions that produce furfural intermediates, which repolymerize into aromatic clusters. Due to the high concentration of aromatic clusters, created by aromatization reactions during the carbonization process, the mixture reaches the critical saturation point which leads to burst nucleation. Nuclei expand by linkage of present chemical species to the nuclei surface. This nucleation process leads to oxygen containing functional groups being on the outside of the microsphere, hence the hydrochar particles having a hydrophilic outer shell and a hydrophobic core.[36]

1.6.3 Activated Carbons in Supercapacitor Electrodes

As described by the capacitance equation (**equation 1** in section **1.2.2**), large electrode surface area gives higher capacitance. Therefore, activated carbons, with surface areas of over 3000 m^2g^{-1}, are the perfect material for supercapacitor electrodes. However, as stated in **1.3**, capacitance is limited to 10-20 % of the theoretical capacitance by the existence of micropores, which are too small for the electrolyte to access and also are too small for a double-layer to form.[37][38] To fully maximise the electric double-layer mechanism in EDLCs or hybrid supercapacitors, the pore size distribution, specific surface area and wettability behaviour of activated carbon electrodes must all be taken into account.[39][40][41]

1.6.4 Activated Carbons as Hydrogen Storage Materials

Because of their adjustable PSD, large surface area, and variety of possible precursor, KOH activated carbons are of huge interest as a candidate for hydrogen storage for hydrogen fuel cells and stations. A number of researchers studied the adsorption of H_2 in anthracite and pitch derived KOH activated carbons and found the maximum uptake to be 1.2 wt%.[42][43][44] These studies were carried out at room temperature and pressure, and when compared with studies at cryogenic temperatures (77 K), the activated carbons absorb much more H_2 (up to 6.0 wt% by Maxsorb-3000).[45] From these findings, it is shown that activated carbons ability to store H_2 is seriously affected by temperature, therefore it is the goal of most researchers to increase the hydrogen uptake at higher operating temperatures. Heterogenous dopants have been shown to greatly increase the H_2 uptake of activated carbons, specifically nitrogen, boron and transition metals. Nitrogen has been shown to improve the surface chemical reactivity by enhancing the π-bonding and basicity of graphene-like substrates.[46][47] Furthermore, nitrogen increases the conductivity of the substrate by contributing to the electron density of the substrate.[48]

1.6.5 Metal Doping of Activated Carbons

As stated earlier, transition metals can be used as dopants in carbons to improve their hydrogen uptake. A mechanism proposed by S. Khoobiar in 1964 and explored by Yang *et al* in 2006, suggested that hydrogen spillover is a possible route for higher hydrogen uptake.[49][50] The proposed mechanism of hydrogen spillover is catalysed by transition metals such as Pt, Pd, Ru or Ni, and begins with dissociation of H_2 onto the metal surface. It is then followed by migration of hydrogen atoms from the metal catalyst surface to the substrate surface. Hydrogen atoms then diffuse over the substrate surface and recombine into molecular hydrogen. The mechanisms individual steps have been studied extensively however and it is clear that the mechanism is not well understood yet. For example, quantum simulations ran by Hen *et al* show that migration along graphene-like surfaces needs high temperatures of around 100 °C, and is simply inefficient at room temperature, however this is not the case.[51]

Transition metal oxides (TMOs) have been shown to exhibit excellent pseudocapacitance, and therefore increase the specific capacitance of hybrid supercapacitors.[52][53][54] This is down to the weakly attached surface ions.[55] Furthermore, if the TMO nanoparticles are between 2 and 50 nm in diameter, then they experience even higher electrochemical performance due to their own high surface area and PSD.[56] Therefore when TMOs are supported on activated carbon electrodes, the composite material exhibits superior electrochemical performance in hybrid supercapacitors, where both pore size matters, because of the electric double layer, and pseudocapacitance, due to better charge transfer between electrolyte and electrode.

1.7 Alternative Carbon-Based Hydrogen Stores

As mentioned earlier, various other forms (allotropes) of carbon can be used to store hydrogen in the right conditions and when doped with various heteroatoms. Carbon allotropes often have the advantage of their uptake capacities easily predictable and their surface area tailorable. However, some allotropes are easier to prepare than others and some need more treatment to increase their hydrogen uptake capacities.

1.7.1 Graphene

Hydrogen storage occurs in carbon-based materials in two ways: physisorption or chemisorption.[57] Physisorption happens between the graphene sheet and molecular hydrogen and the binding is very weak (between 0.01-0.06 eV).[58] Therefore, cryogenic temperatures are needed to maintain the bonds between the surface and the H_2. Chemisorption is a chemical bond between carbon atoms in

the graphene and atomic hydrogen. Chemisorption involves dissociation of the H-H bond and so there is a barrier of roughly 1.5 eV.[57]

Graphene has a surface area of ~2630 m^2g^{-1} and has a theoretical hydrogen uptake capacity of 16.6 wt% (8.3% on each side), which corresponds to a fully saturated sheet of graphene, known as graphane.[59][57] However, in practice and under standard conditions, uptake capacities are much lower (between 0.1-0.7 wt%).[60] Even graphene powder at 77 K exhibits an uptake capacity of 1.2 wt%, and a study by Klechikov et al found a maximum uptake capacity of 4.1 wt% at 77 K, therefore its theoretical uptake capacity is far from its practical uptake capacity.[60][61] Graphene and its analogues can be chemically modified to enhance its uptake capacities, to give functionalised graphene (f-G).[59] Graphene can be doped with various heteroatoms and functional groups containing oxygen, sulphur phosphorus, etc. Graphene and its analogues can also be chemically activated with KOH in a similar way to activated carbons. For example, in a study by Klechikov et al, graphene oxide was activated with KOH to give a material with a surface area of 3000 m^2g^{-1} and a pore volume of 2.2 cm^3 g^{-1}.[62] Furthermore, graphene can be doped with metals such as Li, Ca and Ti, and V.[63][64][65] Graphene can be functionalized with acidic groups such as hydroxyl or carbonyl groups which create defects in the graphene sheet. These defects can be used as adsorption sites for H_2, but they can also be used as nucleation sites for these metal nanoparticles.[66]

1.7.2 Spherical Fullerenes

Fullerenes are effectively a sheet of graphene rolled up into a ball with 12 pentagonal faces and n/2 – 10 hexagonal faces, where n from is C_n.[67] In the case of C_{60} (buckminsterfullerene or buckyballs) it is made up of 12 pentagonal faces and 20 hexagonal faces. Studies by Zhao et al and Yildirim et al showed that C_{60} can be doped with lighter transition metals such as scandium and titanium, but not with heavier metals like manganese and iron.[68][69] In the case of scandium, each atom can bind with 11 hydrogen atoms, 10 of which are in the molecular H_2 form, giving a theoretical uptake capacity of 9 wt%.[67]

1.7.3 Carbon Nanotubes

Single walled carbon nanotubes (SWCNTs or SWNTs) can be thought of as elongated fullerenes that have been capped, hence the informal name of buckytubes.[70] If multiple graphene sheets are rolled up, then a multi-walled nanotube is formed (MWNTs).[71] CNTs fit into one of 3 subcategories: zigzag, armchair, or chiral. The configuration of the CNT is dependent on how the graphene sheet is rolled up and influences the electrical physical properties of the nanotubes.[67] Hydrogen can be stored on both the inside and outside of CNTs and pure nanotubes alone have had reported hydrogen uptake

capacities of up to 10 wt%.[72] Multiple studies on CNTs doped with various metals have been conducted with varying results, this will be discussed later. Similar to graphene, the known structure of the material makes hydrogen uptake and binding energy calculations very easy for CNTs and fullerenes.

1.8 Synthesis, Characterisation and Analysis Techniques of Porous Carbons

1.8.1 Synthesis of Metal Doped Carbons

Metal-doped carbons are typically synthesised using the wet-impregnation technique which is a common technique used to produce metal catalysts with carbon supports. The method is carried out in an aqueous solution in which metal salts, usually nitrates or chlorides, are dissolved.[73] Metal loading is controlled by the concentration of metal ions in the aqueous solution. Despite nitrates being commonly used due to their solubility in water and other polar solvents, they yield catalysts with very poor dispersion.[74] The reason for this poor dispersion is not well understood, however, it is known that using citrate salts or adding viscosity increasing agents to nitrate solutions yields catalysts with high dispersion. Thus, it is suggested that low dispersion is due to redistribution of metal nanoparticles during drying.

1.8.2 Powder X-Ray Diffraction

XRD is a characterisation technique in which a diffractometer produces X-rays with a typical wavelength of 1.5418 Å, characteristic of CuKα emission, in order to identify unknown crystalline materials.[75] Waves are either reflected off the surface of the structure, or they enter the lattice, where they can interfere constructively and destructively depending on the region. This produces bright spots which help put together a picture of the atomic structure in three-dimensional space. Bright spots occur from constructive interference which happens in regions where atoms are arranged symmetrically , with interlayer spacing d, and the path length distance (2dsinθ) is equal to nλ, where n is a positive integer and corresponds to the layer number. This is in accordance with Bragg's Law:

$$2\text{dsin}\theta = n\lambda$$

[Equation 2]

d = interlayer spacing   θ = diffraction angle   n = layer number

Thus XRD can be used to calculate the interlayer spacing as well as the unit cell of the metal nanoparticles decorated on porous carbon materials.

1.8.3 Brunauer-Emmet-Teller (BET) Theory

Developed by Stephen Brunauer, Paul Hugh Emmet and Edward Teller in 1938, BET theory builds upon the theory of gas adsorption on surfaces of materials by Irvin Langmuir, and is the basis for BET analysis.[76] BET analysis is used for the measurement of specific surface area of porous materials and most commonly used probing gas is nitrogen, hence N_2 sorption BET analysis is usually carried out at 77 K. As well as surface area, pore size and pore size distribution (PSD) can be calculated, making BET analysis an important tool for testing the hydrogen uptake abilities of various porous materials. To carry out BET analysis at other temperatures, different adsorbates such as CO_2 or water are used. Assuming the gas behaves ideally, at low to moderate temperatures and pressures the gas adsorbs onto a surface as a monolayer, as described by the Langmuir equation:

$$\theta = \frac{KP}{1 + KP}$$

[Equation 3]

The BET equation builds upon the Langmuir equation (**equation 3**) which does not account for multi-layer adsorption at high temperature and pressures. BET theory makes several assumptions and hypotheses:

- Gas molecules adsorb in layers indefinitely.
- There are no lateral interactions between adsorbed gas molecules.
- Enthalpy of adsorption for the first layer is greater than subsequent layers.
- Enthalpy of adsorption for subsequent layers is equal to the enthalpy of liquefaction.
- The Langmuir equation can be applied to each individual layer.

$$V_{total} = \frac{V_{mono} C (\frac{P}{P_o})}{(1 - \frac{P}{P_0})(1 + C \left(\frac{P}{P_0}\right) - \frac{P}{P_0})}$$

[Equation 4]

$$C = \frac{K_1}{K_L}$$

From BET analysis, an isotherm can be placed into one of six classifications, each of which is characteristic of certain adsorption patterns and porosities.[76]

- Type I isotherms are typical of microporous materials and is initially a linear relation between pressure and gas uptake until it plateaus due to micropore volume limiting uptake. Type I isotherms describe monolayer adsorption.

- Type II isotherms are typical of macroporous or non-porous materials where the pore size is much larger than the adsorbate size. After the initial plateau, uptake steadily rises again which indicates the completion of a monolayer and the start of multilayer adsorption.

- Type III isotherms also indicate macroporous or non-porous materials, due to unrestricted multilayer adsorption, but with the presence of strong lateral interactions between adsorbate molecules in comparison to the enthalpy of adsorption.

- Type IV and V isotherms are characteristic of mesoporous materials, which proceeds by multilayer adsorption followed by capillary condensation, indicated by the hysteresis loop. This effect limits the uptake at high partial pressure. Type IV and V isotherms are analogous to type II and III isotherms, respectively. If capillary condensation in mesopores is reversible then the hysteresis loop is not present in the isotherm which is known as a type IVc.

- Type VI isotherms are characteristic of uniform, non-porous materials. Multilayers adsorb in a step-wise fashion, indicated by the steepness of the isotherm being dependant on the conditions of the system. This step-wise multilayer adsorption usually remains constant for two to three multilayers.
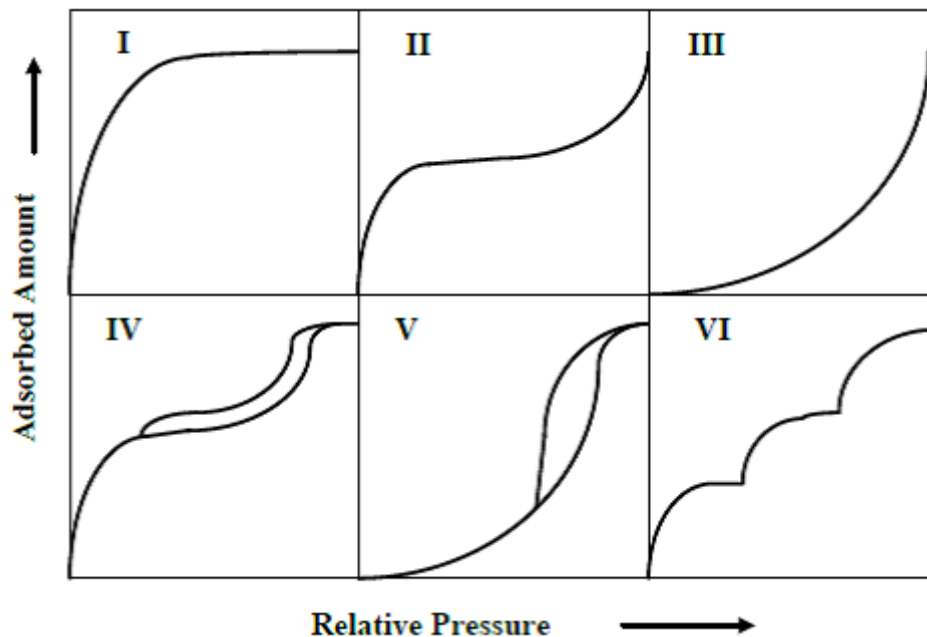

Fig 6. The six different types of sorption isotherm.

Between the relative partial pressure (P/P$_0$) range of 0.05 and 0.35 the isotherm can be plotted as a straight line with the gradient $(C - 1)/(V_{mono}C)$. From this straight line the BET surface area can be calculated, as seen in **equation 5**.

[Equation 5]

$$S_{BET} = \frac{V_{mono} + N_A + A}{M_v}$$

Where A is the gradient of the slope and N_A is Avogadro's number. The Halsey equation can be derived using a t-plot (thickness-plot) to calculate the thickness factor:

$$t = 3.54 \times \sqrt[s]{\frac{5}{ln\frac{P_0}{P}}}$$
[Equation 6]

Note: This equation is for N_2 at 77 K.[77]

From the t-plot y-intercept, micropore volume and micro-/mesopore surface area can be derived from the following equations:

$$V_{micropore} = 0.001547 \times (t - y\ intercept)$$

$$S_{mesopore} = 1.547 \times (t - gradient)$$

$$S_{micropore} = S_{BET} - S_{mesopore}$$

When using BET theory on activated carbons, the external surface area is greatly overestimated due to enhanced adsorption is micropores.[78] Therefore in the presence of microporous activated carbons, to more accurately estimate the external surface area, other methods much be employed, such as the subtracting pore effect (SPE) method.[79] However, in the case of microporous activated carbons for use as hydrogen stores, external surface area is not a necessary standalone value that needs to be understood.

1.8.4 Cyclic Voltammetry (CV)

Cyclic voltammetry (CV) is a method of obtaining an analytes electrochemical properties in solution.[80][81] A standard CV cell consists of three electrodes: working electrode, reference electrode, and counter (auxiliary) electrode. During a cyclic voltammetry trace, the working electrode potential is ramped at a constant rate until the set potential is met, at which point the working electrode potential is negatively ramped. The rate of voltage change per second is known as the scan rate, with units Vs^{-1}. Current at the working electrode is plotted against voltage to produce a cyclic voltammogram.[82] The job of the reference electrode is to measure the potential difference between itself and the working electrode to obtain voltage, where the counter electrode's job is to measure current flowing between itself and the working electrode. Therefore, the surface area of the counter electrode must be higher than that of the working electrode so that it will not being a limiting factor in the kinetics of the reaction. The counter electrode is usually made from an inert material such as

platinum or graphite and does not react with the analyte in solution. In the three-electrode setup, electrodes are not spun, and the solution is not stirred owing to the diffusion-controlled peaks, seen in the voltammogram.

From a cyclic voltammogram, the specific capacitance of the working electrode can be derived from the following equation:

$$C_s = \frac{\int I \, dV}{mv\Delta V}$$

[Equation 7]

Where C_s is the specific capacitance (Fg^{-1}), I is the current (A), the integral is the area under the voltammogram oxidation curve, m is the mass of the active material (g), v is the scan rate (Vs^{-1}), and ΔV is the potential difference of the working electrode (V).[83]

1.8.5 Galvanostatic Charge-Discharge Measurements (GCD)

GCD or also known as chronopotentiometry is a method for evaluating electrochemical parameters of various materials, such as specific capacitance, resistance and cyclability.[80][84] GCD uses the same three-electrode set up as cyclic voltammetry, however current is kept as a constant, and voltage is measured. When current is applied to the system, voltage changes drastically due to ohmic losses.[85] After the initial change in potential difference, the voltage changes more gradually due to mass transport losses, which occur due to a lack of reactant at the electrode surface.[86] Voltage as a function of time is described by the equation:

[Equation 8]

$$V(t) = IR + \frac{t}{C} I(V)$$

[Equation 8]

Where C is capacitance (F/g) and R is resistance (Ω). Therefore, specific capacitance can be calculated via integrating under the GCD curve and dividing by the mass of the active material, arriving at the equation:

$$C_s = \frac{I\Delta t}{m\Delta V}$$

[Equation 9]

2. Project Aims

The aims of this study are to investigate the effects of doping various forms of porous and nano-carbons with different metal atoms when applied to two energy based applications; (i) as electrodes with increased specific capacitance in supercapacitors; (ii) as hydrogen storage materials for a

potential hydrogen economy. Different metals and carbon precursors are compared and contrasted in order to conclude the best material for the application. In the case of supercapacitors, transition metals on graphene are thought of as the future of supercapacitor material. This paper will investigate the potential of both graphene and activated carbons, and aim to identify the best current metal dopants for increasing capacitance. For hydrogen storage, activated carbons are be compared to graphene as well as nanocarbons. Furthermore, hydrogen affinity, increased by metal nanoparticle decoration due to the effects of hydrogen spillover and H_2 binding energy, is also compared between different metals and to the pure carbons.

3. Metal Doped Carbons in Energy Applications

3.1 Electrochemical Applications

3.1.1 M and MO/Activated Carbon Supercapacitor Electrodes

As stated in **1.6.5** transition metal oxides can be doped onto activated carbon-based, hybrid supercapacitors, in order to increase their pseudocapacitance. [52][53][54] Capacitance increases when adding metal oxides to activated carbons (AC) for two reasons; (i) addition of metal oxides introduces pseudocapacitance mechanism, (ii) when heating/annealing the composite, mesopores are introduces into the AC structure, slightly increasing the surface area.[87][88] Despite the second factor increasing the surface area off the base AC, the surface area of the overall composite decreases when metal oxide is added.

Ruthenium Oxide (RuO_2)

The pseudocapacitive behaviour of ruthenium oxide has been a key point in electrochemical studies for the past two decades.[89] Ruthenium oxide is known as a good candidate for pseudocapacitors due to its low resistivity of 3.6×10^{-5} Ω cm, and because it has three accessible oxidation states, therefore making it favourable for electrochemical reactions.[90][91] Early studies by Sato *et al* found that loading coal-based, activated carbon electrodes with 7.1 wt% RuO_2 lead to a 20 % increase in capacitance, with a maximum value of 308 Fg^{-1} for the composite.[87] Later, Nanaumi *et al* found that 3.2 wt% RuO_2 loading onto coal based AC, lead to a 25 % increase in capacitance (324 Fg^{-1}).[88] A lower metal loading giving a higher capacitance increase for the same AC precursor suggests that there is a maximum efficient loading weight between 3.2 and 7.1 wt% RuO_2. This is partially confirmed by Zheng *et al*, who

found that loading 5 wt% RuO_2 loading onto lignite derived AC, gave an increase in specific capacitance of 40.8 %, as well as a specific energy density increase of 39.1 %.[92] This volcano plot-style behaviour of capacitance when metal loading is due to the negative effect of metal nanoparticles forming large clusters on the activated carbon, blocking the pores and hence lowering the surface area, outweighing the positive effect of the introduction of pseudocapacitance. Jang *et al* confirmed via galvanostatic charge-discharge measurements, that the more metal oxide that is doped onto AC, the higher the ohmic voltage drop.[93] Ohmic voltage drop results in a sizeable difference between the potential at the electrode and the overall potential of the system. This is possibly due to the pore narrowing, which increases electrolyte resistance, and therefore limits ion diffusion.[91]

To overcome the drawbacks of pore narrowing, AC electrodes can be electrochemically doped with RuO_2 films, rather than using the traditional wet impregnation method, as demonstrated by Sieben *et al* in 2013.[94] With activated carbon cloth/felt as the pristine electrode, three electrodeposition methods were employed to deposit a layer or RuO_2: Chronoamperometry, chronopotentiometry (GCD), and cyclic voltammetry (CV). The benefit of using electrodeposition techniques over wet impregnation, is that a three-dimensional network of nanoporous RuO_2 film is deposited on the AC, rather than clusters of nanoparticles. This means there is a high degree of oxide utilisation, with a lower degree of pore blocking. Furthermore, the amount of RuO_2 film deposited is highly controllable via electrochemical parameters such as potential difference and applied current.[95][96] The largest increase in capacitance was seen when using CV as the electrodeposition method, with capacitance values between 160 and 180 Fg^{-1} (corresponding to 82 and 100 % increases, respectively).[94] The use of AC cloth over AC powder also has its own benefit, as non-conductive binders are not necessary in the system to overcome the contact resistance of the electrode.

Manganese Oxide (MnO_2)

Manganese oxide is less preferable to ruthenium oxide as it has poor electrical conductivity in comparison. However, manganese is much more abundant that ruthenium making it an environmentally and economically more viable option.[91] Therefore, since manganese-based composites cannot reach the high capacitance of ruthenium oxide composites, research is focused on efficiency and environmental friendliness of the composites. The lower capacitance is evident in studies by Lee *et al*, who doped manganese oxide onto activated carbon aerogel (ACA) at 7 % loading, and found a maximum specific capacitance of 168 Fg^{-1}.[97] This is much lower compared to the specific capacitance of some RuO_2-AC. The majority of studies on MnO_2/AC composites, explore the retention of capacitance over a number of charge/discharge cycles. Ren *et al* used activated biochar, derived from Paulownia flower, a common flower in mainland China and southeast Asia, and used

electrodeposition for the doping of MnO_2 with various ratios.[98] Therefore making the composite very economically reproducible. This particular biomass derived carbon was found to have particularly large PSD, indicated by the presence of a faint hysteresis loop and an increase in adsorption around relative pressure of 1, in the N_2 sorption isotherms (see **fig 7**). These factors suggest there is a small amount of interconnected meso- and macropores as well as a large amount of micropores. A large PSD can be beneficial in electrochemical applications, unlike hydrogen storage, as micropores and mesopores increase the EDL capacitance due to the larger surface area, while interconnected macropores allow a shorter diffusion pathway for electrolyte ions. However, the effect of surface area does not dominate the electrochemical performance of the composite, evident by the largest surface area belong to MnO_2-AC_4, while the best electrochemical performance being exhibited by MnO_2-AC_3, with over 92 % of the specific capacitance remaining after 1000 charge-discharge cycles.[98] Choi *et al* found that MnO_2/AC exhibited an acceptable capacitance of 60.3 Fg^{-1} at 1 Ag^{-1}, and 99.6 % of the specific capacitance was retained over 5000 charge-discharge cycles. When using mesoporous polyaniline (PANI) as the base for MnO_2 doping, as much as 84 % of the specific capacitance is retained after 10,000 charge-discharge cycles.[99]
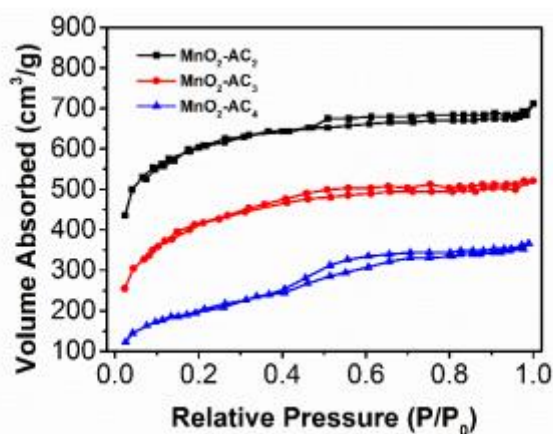
Fig 7. N_2 sorption isotherm of MnO_2/AC

*Nickel Oxide (NiO)*

Like ruthenium oxide, nickel oxide is highly conductive and therefore it exhibits strong pseudocapacitive behaviour.[91] In an early study by Yuan *et al*, it was found that adding 4 wt% NiO onto AC via incipient wetness impregnation, lead to a roughly 7.5 % decrease in surface area, but at the same time, a 10.9 % increase in specific capacitance (175 Fg^{-1} to 194 Fg^{-1}).[100] This increase in capacitance with decrease in surface area indicated that the pseudocapacitance introduced by NiO is a more substantial influence on capacitance, than the decrease in surface area due to the

agglomeration of NiO nanoparticles. Li *et al* discovered that doping 4 wt% NiO, in the form of basic nickel carbonate (BNC), onto sargassum-based AC, lead to a 34.7 % increase in capacitance at 0.1 Ag^{-1}.[101] When loading BNC onto AC, capacitance increases sharply at first but caps off at 4 wt%, due to the negative effect of surface area decrease having more of an impact on specific capacitance, as seen in **table 3** and **fig 8**.

AC/Ni Composite	Specific Capacitance (Fg^{-1})	% Increase in Specific Capacitance
AC	265	n/a
AC/Ni-1	295	11.3
AC/Ni-1.5	333	25.7
AC/Ni-2	355	34.0
AC/Ni-4	357	34.7

Table 3. Specific capacitances of NiO/AC composites with different concentrations of NiO.
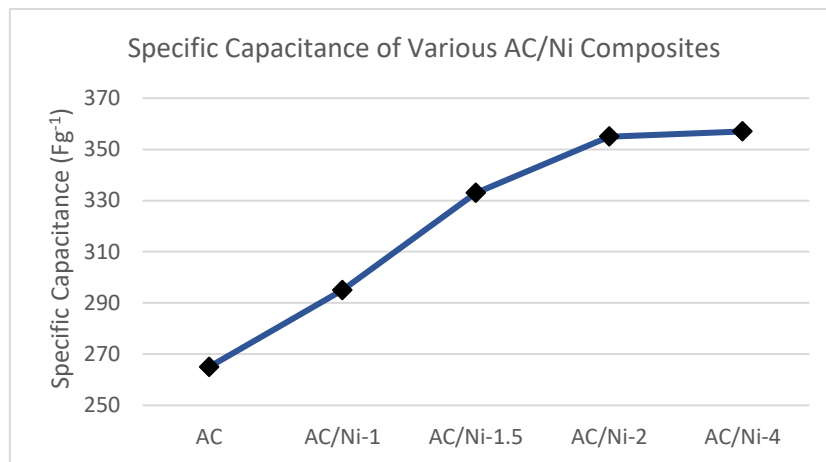
Fig 8. Increase in capacitance levels off at higher NiO concentrations.

When used in an asymmetric capacitor set-up, that is AC/Ni-x as the positive electrode and AC as the negative electrode, charge-discharge efficiency decreased with increasing metal loading (AC/Ni-1: 72.6 %, AC/Ni-2: 53.8 %). A possible reason for this is increasing BNC concentration introduced more impurities into the system which irreversibly react with both the AC and the AC/Ni electrodes.[101] Despite this, significant capacitance retention of 83.5 % is seen over 10,000 charge-discharge cycles.

NiO/AC composites also tend to show good dispersion of NiO nanoparticles when using the wet impregnation method, thus preventing agglomeration and consequently, lower surface area and EDL capacitance.[102] Lee *et al* found that a ratio of 20:1 (NiO:AC), gave the composite electrode a 530 % increase in capacitance on the pristine AC electrode, and a 40 % increase on the NiO electrode, with a maximum capacitance of 624.2 Fg^{-1} at 1 Ag^{-1}. This is possibly due to the pores of the NiO being used as channels for ion movement, and so the AC being used as an EDL capacitance enhancer, rather than the NiO being used as a pseudocapacitive enhancer for the AC.

Iron Oxide (Fe$_3$O$_4$)

Studies carried out by Xie and Zhao *et al*, demonstrated that iron oxide composites have high theoretical specific capacity when used in Li-ion batteries.[103][104] Therefore, along with the benefits of being the earth's second most abundant metal, making it very cheap, and the process of obtaining from ore having low environmental impact, iron oxide composites have been a large area of focus in the field of supercapacitors. Park *et al* found that doping commercially purchased activated carbon with ~12 wt% Fe$_3$O$_4$ gave a maximum specific capacitance of 131 Fg^{-1}, when calculated using GCD.[105] When using CV, the specific capacitance was 101 Fg^{-1}, but both correspond to a roughly 70 % increase on the pristine AC sample. Rodrigues and co-workers calculated a 119 % increase on pristine AC when doping Fe$_3$O$_4$ onto activated carbon felt (ACF), with a specific capacitance value of 237 Fg^{-1} at 0.2 Ag^{-1}.[106] Iron oxide composites tend to show an excellent capacitance retention. Rodrigues *et al* reported a retention of 97 % after 3000 cycles, while Park *et al* found a capacitance increase after 10000 cycles, giving a retention of 105 %.[105] This increase is attributed to two factors; (i) during the cyclic diffusion process, more active material is dispersed onto the electrode over time therefore pseudocapacitance increases; (ii) as the electrode absorbs more ions into the bulk, cyclic diffusion leads to an increase in surface area and pore volume, therefore increasing EDL capacitance.[107] However, Jiang *et al* recorded a 72.6 % retention after 1000 cycles when Fe$_3$O$_4$ was anchored to hemp-straw derived activated carbon (HAC), indicating that this effect does not work for all Fe/AC composites.[108]

A significant number of studies on Fe/AC composites have explored the use of alternate or modified dispersion techniques, instead of the common wet impregnation method used, in an effort to reduce nanoparticle agglomeration and change the morphology of iron oxide clusters. One such method is using liquid phase plasma (LPP) to synthesise and disperse metal oxide nanoparticles.[109][110] When used for the construction of metal oxide composites in EDLCs, the LPP method has a major benefit of being a simple, one-step synthesis, as well as not requiring any reducing agent.[111] Lee *et al* used the LPP method to disperse iron oxide nanoparticles of sizes between 40 and 100 nm onto N-doped AC, and found that composite (designated IONCC-x) surface area did not reduce as much as composites

synthesised by wet impregnation.[112] This however, did not have a strong effect on specific capacitance or capacitance retention, as the maximum capacitance was 127.11 Fg^{-1}, exhibited by IONCC-10, which has a capacitance loss of 10.11 % over 300 cycles. Iron oxide crystal structures have been found to change when the concentration of reducing agent used after wet impregnation is altered.[113] This is important because the crystal structure of iron oxide can significantly affect the capacitance of the composite, for example the specific capacitance of Fe_3O_4 is three times higher than that of Fe_2O_3, however, both forms of iron oxide coexist naturally during Fe_3O_4 synthesis.[114] Oh and colleagues found that an optimum concentration of reducing agent formed Fe_3O_4 clusters on activated carbon without the coexistence of Fe_2O_3.[113] Using hydrazine as the reducing agent, it was found that 5 mL of hydrazine fully reduced Fe_2O_3 to Fe_3O_4. The specific surface area of the FeO/AC composites did not change despite the change in crystal structure, furthermore, the specific capacitance was increased from 99.6 Fg^{-1} to 168.5 Fg^{-1} at 2 Ag^{-1}, from the pristine AC. Despite FeO/AC composites having excellent capacitance retention, all while being cost and environmentally friendly, they often exhibit non-optimal capacitance, due to iron oxides low conductivity. It is widely agreed that to obtain exceptionally high capacitance, iron oxide should be mixed with more conductive metals such as nickel or tin.[91][115]

Mixed Composites (Ni-Co, Ni-Mn, Fe-Mn)

As suggested by Wu *et al*, iron oxide composites should be mixed with more conductive metals in order to increase the exhibited specific capacitance.[115] A maximum specific capacitance of 33 Fg^{-1} using a two electrode measurement was exhibited by Fe_3O_4-SnO_2/AC, however, the optimal loading of Sn in the composite is not stated. Ki *et al*, investigated the addition Fe oxide and Mn oxide at varying concentrations and exposure times, to activated carbon via the liquid phase plasma (LPP) method.[116] At a CV scan rate of 10 mVs^{-1} the best specific capacitance (25.75 Fg^{-1}) was exhibited by composite labelled I1M10-90, which had a ratio of Fe:Mn of 1:10, and a plasma exposure time of 90 minutes. This corresponds to a 5 % increase on the bare AC sample. It appears that increasing Mn concentration and exposure time increases specific capacitance, due to Mn having better pseudocapacitive properties, and there being a larger concentration of metal nanoparticles on the AC surface. However, with such low concentrations of iron oxide, the main benefits of being cheap and environmentally friendly are effectively lost.

Chang *et al* studied the effect of doping different amounts of nickel-cobalt bimetallic oxide onto palm shell derived activated carbon.[117] Using CV, at a scan rate of 4 mVs^{-1}, 50 wt% loading exhibited the highest capacitance of 59 Fg^{-1}, over three times the value of the unloaded AC. The composite showed good capacitance retention of 86.7 % over 1000 charge-discharge cycles. An oversight of the study

was that the ratio of Ni:Co in the composite not explored, and likely has a large effect on the specific capacitance. In a similar experiment, the use of liquid phase plasma (LPP) to deposit Ni and Co oxides onto YP-50F commercial activated carbon, to produce nickel-cobalt oxide activated carbon composites (NCOCC), was explored by Lee and co-workers.[118] Capacitance increased from 24.67 Fg^{-1} to 27.23 Fg^{-1} when AC is loaded with Ni and Co oxides at a Ni:Co ratio of 1:1 (NCOCC-55). Other ratios of Ni:Co were examined (9:1 and 1:9), and both gave lower capacitances of 24.47 Fg^{-1} and 23.89 Fg^{-1}, respectively. While these figures initially appear relatively low, the scan rate used was 50 mVs^{-1}, which is much higher than any other study mentioned in this review. The NCOCC-55 also had an excellent capacitance retention of 93 %. A large overlook by these studies is the need to keep materials environmentally and economically friendly, as the use is to replace fossil fuels with a more ethical and sustainable alternative. Therefore, the use of cobalt oxide is arguably unethical and unsustainable as the majority of the worlds cobalt supplies come from mines in the DRC, a severely politically unstable country, and in some cases human rights abuses occur.[119]

3.1.2 M and MO/Graphene Supercapacitor Electrodes

Similarly to activated carbons, graphene exhibits high EDL capacitance due to its large surface area, and its specific capacitance can be improved by doping with pseudocapacitive materials, for example, transition metal oxides (TMOs) or transition metal dichalcogenides (TMDs). Furthermore, undoped graphene exhibits excellent electrical and thermal conductivity, flexibility, a tuneable band gap and mechanical strength.[120-123] It is also possible to modify graphene easily due to the reactive nature of the sp^2 carbons. Work on TMO doped activated carbons and graphene has concluded that mixed-valence, bimetallic oxides provide a much greater increase in capacitance compared to single TMOs. Based off work on MnO/graphene by Meng *et al*, Wu and colleagues synthesised a novel MnCo$_2$O$_4$/nanographene material in an attempt to further increase capacitance.[124][125] The addition of cobalt increases conductivity and therefore pseudocapacitance, as well as providing additional valence states. Graphene is in the form of a 3D macroporous electrically conductive network (MECN), in order to further increase ease of ionic transportation.[126] To further overcome the ionic transport limits and volume expansion during charge-discharge cycles, experienced by current MnCo$_2$O$_4$ composites, MnCo$_2$O$_4$ nanoarrays are grown on the inner and outer surfaces of the nanographene by self-branching. The maximum specific capacitance of the MnCo$_2$O$_4$/MECN composite was 541.2 mAh/g. The larger specific capacitance compared to individual Mn$_3$O$_4$ and Co$_3$O$_4$ nanoparticles and nanosheets at nanographene is because of the larger surface area exhibited by MnCo$_2$O$_4$/MECN. The major failure of this study was that despite noting that change in metal oxide composition can vastly alter the electrochemical properties, the optimal loading of Mn and Co is not explored. Furthermore,

capacitance values are noted in mAh/g, which due to the pseudocapacitive nature of the material, it is difficult to convert into Fg^{-1}, the standard unit of specific capacitance. Therefore it is hard to compare these results to other studies.

Yang *et al* discovered that using the hydrothermal method to deposit Co_3O_4-NiO onto graphene oxide (GO) resulted in a material with a specific capacitance of 883 Fg^{-1} at 1 Ag^{-1}.[127] This is an exceptionally high value when compared to NiO@AC, which gave a maximum specific capacitance of 357 Fg^{-1} at 0.1 Ag^{-1}. Sarwar *et al* explored the use of TMDs as dopants for graphene, compared to other nanocarbons. $MoTe_2$ on graphene using microwave heating exhibits excellent specific capacitance of 434 Fg^{-1} at 1 Ag^{-1}.[128] However, pure nanosheets of $MoTe_2$, built via colloidal chemical synthesis, exhibit a specific capacity of 1393 Fg^{-1} at 1 Ag^{-1}, suggesting that the graphene support hinders the $MoTe_2$. None the less, the vast majority of TMO and TMD doped graphene electrodes exhibit specific capacities that greatly outshine their activated carbon counterparts, confirming that graphene is more likely the future of supercapacitor electrodes.

3.2 Hydrogen Storage

3.2.1 M/Activated Carbon H_2 Stores

Based on work on SW/MWNTs and carbon nanospheres by Park, Mu and Lueking *et al*, multiple groups have looked into the effects of doping activated carbons with various metals, namely palladium and platinum.[129][130][131]

Palladium and Platinum

Mu *et al* initially reported an optimum platinum loading for hydrogen storage on etched CNTs of 5.7 wt%. Park *et al* recorded an optimum loading value of 4 wt% of platinum on MWCNTs. Based off these results, Aboud *et al* investigated the effects of noble metal (Pd, Pt) doping on activated carbons derived from local waste.[132] Firstly, XRD was carried out to find the nature of the Pd and Pt in the activated carbon. It was concluded that both Pd and Pt were in the FCC (face centred cubic) form when decorated in activated carbon. This was confirmed by Bader *et al* in a study on the effects of noble metals on activated carbons.[133] When impregnated into activated carbons, Pd tends to agglomerate and form large clusters of ~100 nm. Whereas Pt forms uniformly dispersed ultra-small nanoparticles of ~3 nm.[132]

Due to the ability to use almost anything carbon based as a precursor for activated carbons (AC), uptake capacity results tend to differ between studies, however clear patterns emerge. Isotherms of

excess hydrogen (wt%) vs pressure (MPa) are used to calculate the effect of doping and of surface area.[133] In all studies, cryogenic temperature isotherms of AC-Pd and AC-Pt were type I isotherms (see **fig 9**). This type of isotherm indicates that the hydrogen molecules adsorb as a monolayer, and so the adsorption maximum is limited by the micro/mesopores filling up.[132] In contrast, there is a linear relationship between excess hydrogen and pressure when samples are hydrogenated at 298 K (see **fig 10**). This is in compliance with Henry's law which states that concentration of gas is proportional to its partial pressure.[134] At room temperature, both Aboud and Bader groups found that doping with palladium and platinum increased the H_2 uptake capacity by small amounts. Aboud *et al* had an activated carbon with an excess uptake of 0.24 wt%, and found doping with Pd increased the value to 0.25 wt%, and doping with Pt increased it to 0.26 wt%.[132] Meanwhile, Bader *et al* started with an excess hydrogen uptake of 0.45 wt%, Pd gave an increase to 0.52 wt%, and Pt gave an increase to 0.53 wt%.[133] Both studies confirmed that at 298 K, Pt is the better dopant for activated carbons. This is unexpected as previous studies show that Pd-anchored carbons have a higher uptake capacity than any other material.[135][136] However, the thermodynamically favourable formation of palladium hydride is counterbalanced by the size of the Pd nanoparticles.[132] All increases can be attributed to the hydrogen spillover mechanism, and not to the surface area of the porous carbon.[49][50][133] This is because the metal nanoparticles have a lower surface area than the activated carbons. At 77 K and at higher pressures, Aboud *et al* actually found that doping with Pd and Pt very slightly decreased the excess hydrogen uptake when compared to the pure activated carbon (Pd: -0.01 wt%, Pt: 0.02 wt%).[132] This is because the surface area of the activated carbon is the dominating effect on H_2 adsorption, as the system is at the saturation point. Therefore, the addition of metal nanoparticles lowers the surface area by blocking micropores, and the spillover is counteracted.
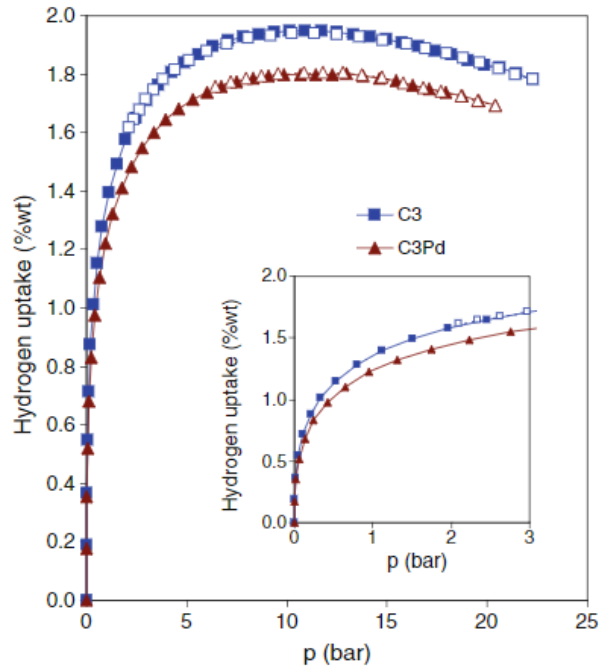
Fig 9. Type I isotherm of hydrogen uptake in doped and pure forms of CMK-3 mesoporous carbon
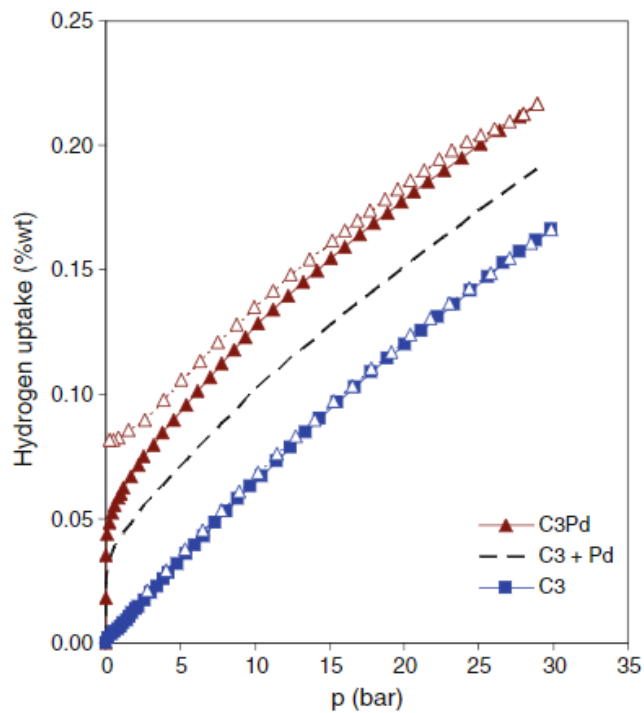
Fig 10. Linear relation between hydrogen uptake and pressure in doped and pure forms of CMK-3 mesoporous carbon

Li *et al* explored the effect dispersing metal nanoparticles uniformly across the carbon surface via a modern technique called plasma-assisted reduction.[137] This method aimed to enhance the efficiency of the metal catalysts for dissociation of hydrogen spillover. Plasma reduction produces highly dispersed nanoparticles of uniform sizes, however like hydrogen spillover, the mechanism is not well

understood. In the study by Li *et al* Pt was used as the dopant and experiments were carried out at room temperature and 100 bar. Using platinum as the dopant, assisted by plasma reduction, a hydrogen uptake capacity of 0.8 wt% can be achieved, compared to the ~0.27 wt% of the pure activated carbon.[137] This gives a 3-fold increase in uptake capacity, whereas Bader *et al* only increased the hydrogen uptake by 17 % at 298 K, using the traditional wet impregnation method.[133]

Nickel

In the same study that explored effect of noble metals by Bader *et al*, nickel, as well as other transition elements were impregnated into the activated carbon. Nickel, when doped into carbon, forms particles of similar size to palladium (~100 nm).[132] However, unlike palladium, nickel forms smaller, more dispersed nanoparticles, whereas Pd tends to agglomerate. This is significant as dispersion and metal particle size both have an effect on spillover.[133] As like Pd and Pt, Ni decorated carbons have a lower surface area than the pure form as pores are blocked by the metal nanoparticles.[138] And such, because of this, only at moderate temperatures does impregnation of Ni have a positive effect on hydrogen uptake. Zeiliński *et al* investigated the effect of nickel acetate ($Ni(CH_3COO)_2$) vs nickel nitrate ($Ni(NO_3)_2$) as catalysts supported by activated carbons at different loading weights, designated xNi/AC-A and xNi/AC-N respectively, where x is the amount of metal loading.[138] As with Pd and Pt, adding too much Ni will block pores and reduce specific surface area so much that hydrogen uptake decreases with higher metal loading. At lower pressure (20 bar), the nature of the nickel precursor does not have an effect on the hydrogen uptake. This is because the precursor has little effect on specific surface area. However, at higher pressure (30 bar), using nickel acetate lowers the hydrogen uptake of 1 Ni/AC, as seen in **fig 11.** For nickel doped activated carbons, the highest hydrogen uptake capacity is for 1 wt% nickel loaded AC, as long as the pressure is high enough to observe the spillover phenomenon. 1 Ni/AC-N achieves a hydrogen uptake of 0.53 wt% which is over 5 times more than the pure activated carbon (0.1 wt%). So, while the hydrogen uptake value is lower than that of Pt doped carbons, assisted by plasma reduction, the increase from the pure form of the activated carbon is much higher. Furthermore, pressures used by Li *et al* were 70-80 bar higher than that of Zeiliński *et al*, suggesting that using a different activated carbon precursor with a nickel catalyst could produce a material with even more exceptional hydrogen uptake at room temperature.[137][138]
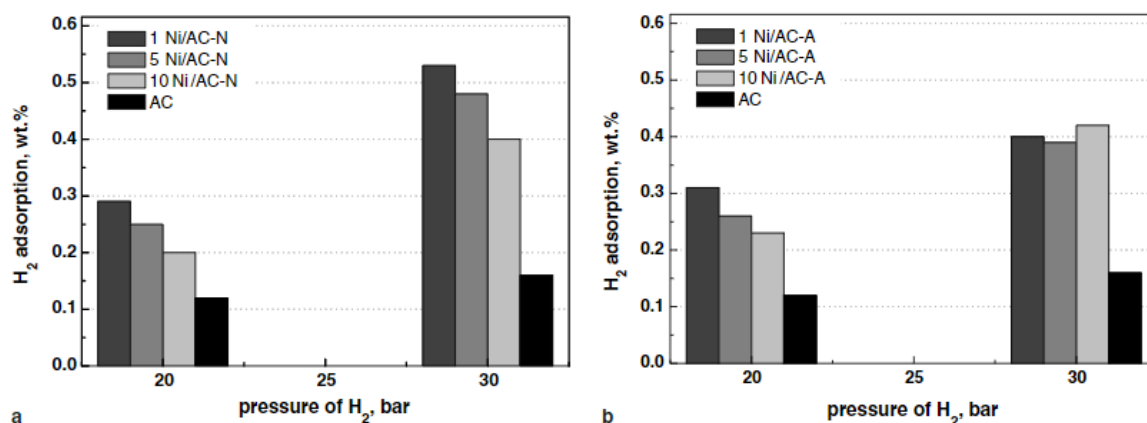
Fig 11. Nickel doped activated carbons at two different pressures with two nickel precursors.

Alkali Metals (Li and K)

Inspired by the studies of Amiel and Legrand *et al* on intercalation of alkali metals in graphite, Saha and colleagues investigated the effect of doping polyfurfuryl alcohol-derived activated carbons (PFAC), with lithium and potassium.[139][140][141] Alkali metals do increase hydrogen uptake capacities of porous, non-polar molecules, but not in the same way as transition metals. Transition metals increase hydrogen uptake by the spillover phenomenon and forming hydride bonds on the metal nanoparticle surface.[49][50] Comparatively, alkali metals increase hydrogen uptake by increasing the charge density of the sp^2 carbon matrix, much like heteroatoms such as nitrogen and oxygen.[141] As with transition metals, alkali metal doping experiments at cryogenic temperatures (77 K) produces type I isotherms typical of microporous materials with a narrow pore size distribution.[132][141] And experiments at moderate temperatures produced linear relations between pressure and hydrogen uptake. As with transition metals, K and Li decrease surface area and lower pore volume (7.8 Å to 5.7 Å and 5.5 Å) by blocking micropores. Therefore, the polarizing effect must be enough to counteract the decrease in hydrogen uptake from the decrease in surface area. At all pressures and temperatures, Saha *et al* found that Li doped activated carbons were inferior to pure activated carbons with respect to hydrogen uptake. A study by Minoda *et al* showed that activated risk husks doped with Li had a 5 % decrease in hydrogen uptake, but a hydrogen adsorption affinity increase of +0.21 kgm^{-3}.[142] This indicates that the effect of Li doping varies with activated carbon precursor. Similarly, K-doped activated carbons show inferior hydrogen adsorption compared to the pure forms at moderate temperatures. However, at temperatures lower than 273 K, K-doped carbons showed an increase in hydrogen adsorption. A study by Zhang *et al*, also using PFA as the carbon precursor, showed that using very small amounts of potassium (0.2 wt%) can increased the hydrogen uptake by up to 35% at near room temperature.[143] With high metal loading, adsorption is only increased by about 8%. This is much less of an increase upon the pure activated carbons compared to nickel and platinum doped

carbons. The major limitation with alkali doped carbons is the small number of appropriate adsorption sites, not the weak interaction between the surface and H_2, like in transition metal doped carbons.[143]

3.2.2 M/Graphene and M/Graphene Oxide H_2 Stores

A major problem with doping metal atoms into activated carbons is that the metals, particularly Pd, tend to agglomerate, due to the favourable metal-metal interaction over the metal-substrate interaction, and form larger clusters than are needed (100 nm or even bigger).[132] These larger clusters can block the micropores and greatly reduce the specific surface area, which can be a large limiting factor for hydrogen adsorption. This problem can be overcome by anchoring small metal clusters to defects in the carbon network, which is much easier to do in graphene for two reasons. Firstly, the structure of graphene is much more well-known than the structure of any activated carbon due to its simplicity and two-dimensionality, therefore studies can be conducted computationally. Secondly, defects in graphene, namely mono- and divacancies, increase the adsorption energy of metal clusters over the cohesive energy of the metal.[144]

Noble Metals (Pd, Pt)

López *et al* investigated the effect of doping graphene monovacancies with Pd atoms and small Pd clusters and found that the binding energy of Pd to defects is 0.21 eV, which is the same value for the desorption energy of H_2 from Pd.[145] However, the desorption energy of palladium hydride complexes from monovacancies in graphene is 4.22 eV, therefore, the desorption of the complex from the defect does not compete with the desorption of H_2 from Pd. This is not the case for pristine graphene, and so the presence of defects in the graphene sheet is imperative. The binding energy of H_2 onto Pd anchored to defects on graphene sheets is 0.21 eV, which is smaller than the target binding energy range of 0.3-0.4 eV created by Li *et al*, for reversible sorption of hydrogen on graphene at moderate temperatures.[146] This is compared to a binding energy of H_2 on Pd decorated pristine graphene of 0.96 eV.[144] So, while Pd in defects has a smaller binding energy, making it less suitable for moderate temperatures, it is not bound too strongly. Parambhath and colleagues conducted a study into the effect of Pd and N co-doped graphene and found a maximum uptake capacity of 4.4 wt% at 298 K and 40 bar.[147] This is in comparison to Pt doped carbon which achieved a maximum uptake of 0.8 wt% at 100 bar.[137] This value is achieved by the role of nitrogen, donating electron density to the graphene sheet, complementing the effect of Pd doping. It is discussed that the low binding energy of H_2 to Pd actually benefits the adsorption of hydrogen as it more easily allows adsorption and migration to the metal support via spillover.[49][50][147]

Divya P. and S. Ramaprabhu studied the effect of platinum anchored, hydrogen exfoliated graphene (HEG). Graphene oxide is exfoliated by heating up to 250 °C in the presence of H_2 to produce HEG.[148] Pt-doped HEG can store up to 1 wt% hydrogen at 20 bar, which is twice as much as undoped HEG. With respect to Pt-doped activated carbons , assisted by plasma reduction, Pt-HEG has a 0.2 wt% higher uptake capacity.[137] However, Pt-AC increases the hydrogen uptake 3-fold compared to the pure activated carbon. Comparatively, Jung *et al* created a Pt decorated graphene foam using "bio-inspired" polydopamine.[149] The Pt decorated graphene foam had a hydrogen uptake of 1.10 wt% at 298 k and 100 bar. It was found that 71% of hydrogen on Pt-HEG is stored on the graphene sheet, due to hydrogen spillover.[148] Therefore, for platinum doped carbon based hydrogen stores to meet the DoE targets, Pt loading must be optimised.

Transition Metals (Sc, Ti, Ni)

As discussed earlier, it is well known that the addition of transition metals (TM) into graphene and other carbon based systems can improve upon the hydrogen uptake capacities, but it is limited by the agglomeration of the metal atoms due to the strong cohesive binding energies. Therefore, the main area of study regarding TM doped into graphene is attempts to maximise H_2 adsorbed onto metal atoms without them binding to each other.

Based on previous work by Chen *et al*, regarding the doping of yttrium onto porous graphene (PG), Yasareh *et al* investigated the hydrogen uptake ability of scandium doped porous graphene.[150][151] The most stable position for Sc on PG is in the middle of a carbon ring, adjacent to the vacancy, as seen in **fig 12**. As with Pd and Pt, the adsorption energy of Sc on porous graphene is higher than that of Sc on pristine graphene, and so the desorption of ScH_2 does not compete with H_2. Hydrogen prefers to adsorb symmetrically round the Sc atom, therefore, due to repulsive forces a maximum of 4 H_2 molecules can bind to Sc-PG.[151] A fifth H_2 bonds into an upper layer above the Sc atom with a small binding energy of ∼0.15 eV, which is below the 0.2-.07 eV range suggested by the DoE for reversible hydrogen storage.[152] However, Wang *et al* conducted a study into the effect of Sc adsorption onto B-doped PG, and found that a fifth H_2 molecule did not dissociate and had a binding energy of 0.187 eV, which is also below the DoE target.[153] Using B-doped PG, a second Sc atom can be placed adjacent to the first, inside another C ring, rather than agglomerating with the first and reducing the surface area. This increases the number of H_2 molecules on Sc to 12, with an average adsorption energy of 0.225 eV, giving a theoretical maximum hydrogen uptake capacity of 9.13 wt% at room temperature.[153] This comfortably satisfies the DoE target, however the values are theoretical and so the true uptake capacity at room temperature could be less.
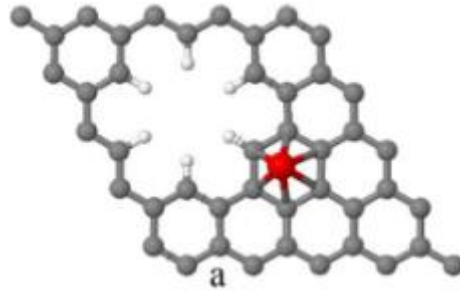
Fig 12. Most stable arrangement of Sc on PG

Wang *et al* studies the use of titanium doped graphene oxide (GO) as a high capacity hydrogen storage-medium.[154] As with any metal atom anchored onto a carbon substrate, the main focus is on preventing clusters from forming, hence the use of graphene oxide over graphene. Oxygen atoms on the surface provide sites for the Ti atoms to anchor directly. Multiple configurations of Ti on GO exist due to the differing nature of O on GO: O can be O, OH or epoxy.[155] The presence of epoxy on the GO surface results in a reaction between itself and Ti atoms, where the epoxy group is removed from the GO surface and the Ti atom binds directly to the carbon atoms underneath (see **fig 13**). This reaction is unfavourable for H_2 storage applications. To eliminate the reaction the only reasonable solution is to hydrogenate epoxy, however, it has been shown experimentally that hydrogenation of epoxy groups on GO also hydrogenates sp^2 carbon into sp^3 carbon.[155] For these reasons, Ti-doped GO has a relatively lower theoretical hydrogen uptake capacity of 4.9 wt%, when compared to other TM doped graphene materials.[154]
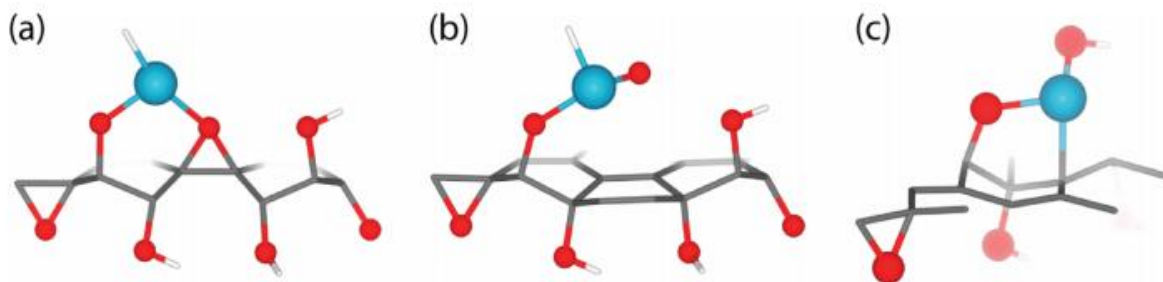
Fig 13. Three stable structures of Ti anchored to GO.

Chu *et al* achieved a theoretical hydrogen uptake capacity of 6.3 wt% when anchoring Ti onto divacancies (DV) in graphene.[156] It was found that the most stable configuration of Ti in the DV was when it was in plane with the graphene sheet. This allowed a maximum of 8 H_2 molecules to adsorb onto Ti (4 molecules on either side of the graphene sheet. A theoretical uptake capacity of 6.8 wt% was calculated by Mashoff *et al* by increasing the active surface of Ti by creating defects in the graphene sheet via nitrogen sputtering.[157]

Cavallari *et al* investigated the catalytic activity of metal clusters anchored to thermally exfoliated graphene oxide (TEGO).[158] When nickel was doped onto TEGO it gave it an uptake capacity of less than 0.5 wt%, which was not a significant improvement upon pristine TEGO. Cavallari *et al* suspected that this was due to an upper hydrogen uptake limit caused by the density of unsaturated defects on TEGO.[158] Gu *et al* studied the hydrogen uptake of co-doped Ni/Al-graphene composites and found a maximum uptake capacity of 5.13 wt% at 373 K, and 5.7 wt% at 473 K.[159] The role of the Ni/Al-graphene composite for hydrogen adsorption is two-fold; Ni is used to dissociate H_2 into H atoms so they can be adsorbed onto Al and graphene via spillover; Al is used to reduce the energy barrier of hydrogen adsorption as it has a theoretical uptake capacity of 10.08 wt%; defects/vacancies in the graphene sheet provide a site for anchoring of metals and further promote hydrogen adsorption.[159] The uptake capacity of the composite being half that of the theoretical uptake capacity of Al shows that Al is not fully optimised on the graphene layer, and that theoretical values are much higher than the real uptake capacities. Furthermore, both Ni-doped graphene materials discussed did not surpass the hydrogen uptake capacities of Ti- and Sc-doped graphene composites, suggesting that Ni is not as good of a dopant as other transition elements.

Alkali Metals (Li, Na, K)

As alkali metals are lighter than transition metals, the gravimetric density of hydrogen on alkali metal-doped carbons is higher. This means alkali metals are a promising candidate for hydrogen storage as they are naturally more weight efficient. Using graphane (hydrogenated graphene) as the substrate, Antipina *et al* found that Li, Na, and K had hydrogen uptake capacities of 12.2 wt%, 10.3 wt%, and 8.56 wt% respectively, all of which have binding energies of $\sim$-0.2 eV/H_2.[160] All of these values comfortably fall withing the DoE requirements, but note that this is under optimal conditions. Li-doped graphane, being the most promising, has an uptake capacity of 9.44 wt% at 300 K and pressures as low as 5 bar. One major limiting factor of alkali metal doped graphene based systems is that metal atoms can become oxygenated and form very strong, effectively irreversible bonds with oxygen molecules, therefore competing with the adsorption of hydrogen. Lee *et al* found that using graphyne over graphene resulted in much smaller binding energies of molecular hydrogen on alkali-metal decorated complexes, especially Li-graphyne.[161] Graphyne is similar to graphene as it is a 2D, one atom thick sheet of carbon, however it is comprised of a mixture of sp^2 and sp^3 carbons, hence there are multiple varieties of graphyne.[162][163] Li-graphyne can store up to 10 wt% hydrogen, making it an extremely promising canditidate for H_2 storage.

3.2.3 M/Fullerene H_2 Store

Carbon Nanotubes (CNTs)

Based off of pure pillared single-walled carbon nanotubes (P-SWNTs) designed by Ye *et al,* which reported a hydrogen uptake capacity of 2-4 wt%, Deng and colleagues synthesized Li-doped SWNTs in an attempt to increase the hydrogen uptake capacity, and meet the DoE requirements.[164][165] An earlier experiment by Pinkerton *et al,* reported a null hydrogen uptake capacity for closed-end Li-doped SWNTs. It was later found that Li-doped CNTs store 99.5% hydrogen on the inside of the tube, therefore H_2 could not access the insides of the CNTs.[166] At a Li:C ratio of 1:6, on un-pillared CNTs, Deng *et al* initially found hydrogen uptake capacities of $\sim$1.2 wt% at 1 bar. This was an improvement upon the 0.005 wt% under the same conditions for P-SWNTs, made by Hirscher and others.[167] However this was not enough to meet the current DoE requirements. It was further investigated to see if increasing the concentration of Li had an effect on the hydrogen uptake. It was found that increasing the ratio to 1:3 and using pillared SWNTs increased the uptake capacity to 6.0 wt% at 50 bar and 25 °C.[165] A study by Rangel *et al* also proved that increasing the concentration of lithium positively correlated with the hydrogen uptake capacities of SWNTs.[168] The nanotube with the highest uptake capacity was C_4Li (7.6 wt%), and was the most heavily doped CNT. In contrast, Wang and colleagues found that there was a concentration of Li that decreased the uptake capacity.[169] This is because at a certain point, the increased binding interaction is outweighed by the decrease in surface area and pore volume that is presented when decorating porous materials with dopants.

Research by Mehrabi *et al* explored the use of multi-walled carbon nanotubes (MWCNTs or MWNTs) doped with transition metals in an effort to increase the uptake capacity.[170] Nickel and palladium were the two chosen metals as seen in **table 4**. It was shown that addition of nickel immediately improved upon the hydrogen uptake. As much as 18.2 wt% Ni atoms increased the uptake by 1.8 wt% compared to pure MWCNTs. Further confirming the work by Wang et al, it was shown that too much dopant can block the nanotubes and decrease the specific surface area, resulting in a lower uptake capacity.[169] Pd is by far the better dopant as with 67% metal loading, the uptake capacity was increased a further 6.5 wt% upon the Ni-decorated MWCNTs. While these values are impressive at first, the experiments were carried out at 77 K, and so the values would surely be lower than that of Li-doped SWNTs.

Sample	Metal Nanoparticle wt%	Hydrogen Uptake Capacity, wt%
MWCNT	0.0	0.3
Ni-MWCNT	18.2	2.1
Ni-MWCNT	25.3	2.5
Ni-MWCNT	35.6	2.3
Pd-MWCNT	67.0	8.6
Pd-MWCNT	69.0	8.6

Table 4 . Uptake capacities of various TM-doped MWCNTs at different loading wt%.

Spherical Fullerenes

One major advantage spherical fullerenes have over CNTs is that there is an established means of easily producing pure fullerenes, unlike pure CNTs, which are difficult to produce with controlled dimensions.[171] However, the binding interactions between H_2 and spherical fullerenes are very weak, and the amount of hydrogen that is able to adsorb onto pure spherical fullerenes is much less than that of pure CNTs.[172] In an attempt to increase the hydrogen uptake of spherical fullerenes, Yildrim *et al* explored the effect of doping transition metals onto C_{60} (buckminsterfullerene).[173] Two factors where investigated; (1) what position on C_{60} provides the best site for metal binding; (2) which transition metal can adsorb the most H_2 molecules. Four binding sites for transition metals were studied as seen in **figure 13**. It was found that early transition metals (Sc and Ti) prefer hexagon (H) sites, also known as hollow sites. Intermediate transition metals (Cr and V) are most stable in the double bond site (D), while late transition metals (Mn, Fe and so on) cannot bind to C_{60} due to the C_{60}TM complexes being very unstable. While Ti is more stable in the H site, it can adsorb more hydrogen in the D site. This is because when bound strongly to the H site, Ti does not have enough charge left to transfer to the antibonding orbital of the H_2 molecules. When in the D site, each Ti atom can adsorb up to 4 H_2 molecules each, and with high metal coverage, $C_{60}Ti_{14}$ can store up to 56 H_2 molecules, which corresponds to 7.5 wt% at moderate conditions.[173]
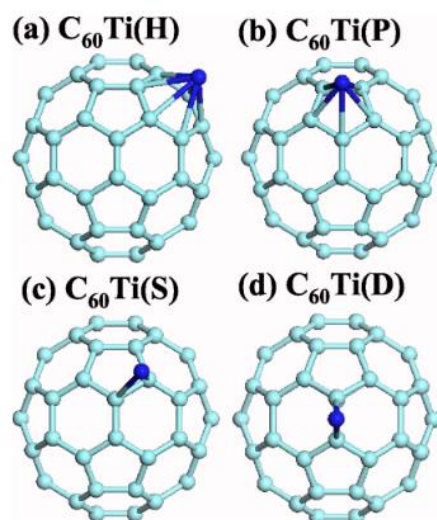
Fig 14. Ti bound to four potential sites on C_{60}: hexagon (H) (a), pentagon (P) (b), single-bond (S) (c), and double-bond (D) (d).

Even when heavier TM can be anchored to C_{60}, the H_2 uptake is much lower than early TMs. For example, Saha *et al* studied the hydrogen uptake capacities of Pd and Ru decorated C_{60} at room temperature and found that both materials produces type III isotherms, indicating very weak energy of adsorption of H_2 molecules.[174] The uptake capacities of Pd-C_{60} and Ru-C_{60} are 0.85 wt% and 0.69 wt% respectively, and while this is an improvement upon the 0.3 wt% exhibited by pristine C_{60}, these values are much less than Sc/Ti doped C_{60}, and do not come close to the DoE requirements. Therefore, heavy transition metal doped fullerenes are much less viable for H_2 storage.

A study by Srinivasu et al explored the use of $C_{24}N_{24}$ fullerenes doped with early transition metals. The somewhat square structure of $C_{24}N_{24}$ forms six N_4 cavities (one on each face), each of which provides a very strong binding site for the TM.[175] Using Sc as an example, each metal atom can bind to four H_2 molecules each, but with a smaller number of binding sites for metal atoms compared to C_{60} fullerene, $C_{24}N_{24}$-Sc has a lower uptake capacity (~5.1 wt% at ambient temperature).

Alkali metals provide a promising alternative to transition metals for use as fullerene dopants. As stated earlier, alkali metals are lighter than transition metals, the gravimetric density of hydrogen in alkali metal decorated C_{60} is higher. Work by Chandrakumar *et al* found that a maximum uptake capacity of 9.5 wt% was possible by high coverage Na-doped C_{60}.[171] In this experiment, a maximum of eight Na atoms were doped onto C_{60}, each binding to six H_2 molecules each. The most stable binding site for Na on C_{60} is in the hexagon (H) site. Therefore, to increase the hydrogen uptake further, Na should be embedded into the pentagon (P) sites. This is possible as work by Palpant *et al* showed that a maximum of 12 Na atoms could be embedded onto C_{60} before clusters form.[176]

4. Conclusions

It is clear that alternative energy stores to replace fossil fuels are far from optimised. However, a large number of promising candidates have been explored. TMOs on activated carbon almost always improve the capacitance by the introduction of pseudocapacitance. More conductive metals such as Ni and Ru have a greater effect on capacitance than metals like Fe and Mn, however, the latter metals are more abundant and cheaper to source. Therefore, it is concluded that a mixture of different metal oxides should be used to maximise specific capacitance of EDL capacitive materials, while keeping construction cheap, if it were to become commercialised. Graphene has presented itself as a superior support for TMOs for use as supercapacitor electrodes as all graphene based TMO doped electrodes have higher capacitances than their AC counterparts.

Even with the addition of various metals and metal oxides, it is still difficult to achieve outstanding hydrogen uptake for carbon based materials at ambient temperature due to the weak bonds formed between the carbon surface and the hydrogen molecules after spillover. Despite this, low loading wt% of metals do improve the hydrogen uptake capacities of porous carbons, as long as they do not reduce surface area too greatly. The most effective metal dopants for increasing hydrogen uptake are metals that introduce the spillover phenomenon, i.e. transition metals. 1-Ni/AC improves hydrogen uptake by over five times as much as bare AC. So while the hydrogen uptake capacities at room temperature do not currently meet DoE requirements, TM doping provides a promising solution for the optimisation of AC based hydrogen stores. CNTs, graphene and fullerenes may appear to outshine activated carbons as hydrogen stores, but in practice their reactivity, stability and difficulty of synthesis make them unlikely candidates for the DoE material for H_2 storage.

5. References

[1] G. Foster and S. Rahmstorf, *Environmental Research Letters*, 2011, **6**, 4402-4404.

[2] IPCC SR15 Summary for Policymakers 2018, p. 7, https://www.ipcc.ch/site/assets/uploads/sites/2/2019/05/SR15_SPM_version_report_HR.pdf, (accessed June 2020).

[3] Oil and petroleum products explained, https://www.eia.gov/energyexplained/oil-and-petroleum-products/where-our-oil-comes-from.php, (accessed September 2020).

[4] M. Asif and T. Muneer, Renewable and Sustainable Energy *Reviews*, 2007, **11**, 1388-1413.

[5] G. Filis, S. Degiannakis and C. Floros, *International Review of Financial Analysis*, 2011, **20**, 152-164.

[6] Lithium Ion technical handbook, http://www.gpbatteries.com/html/pdf/Li-ion_handbook.pdf, (accessed June 2020).

[7] K. Yu, J. Li, H. Qi and C. Liang, *Diamond and Related Materials*, 2018, **86**, 139-145.

[8] H. El Brouji, O. Briat, J.M. Vinassa, H. Henry and E. Woirgard, *Microelectronics Reliability*, 2009, **49**, 1391–1397.

[9] A. Muzaffar, M. Ahamed, K. Deshmukh and J. Thirumalai, *Renewable and Sustainable Energy Reviews*, 2019, **101**, 123-145.

[10] M. Sevilla and R. Mokaya, *Energy & Environmental Science*, 2014, **7**, 1250-1280.

[11] Q. H. Meng, L. Ling and H. H. Song, *Journal of Applied Electrochemistry*, 2006, **36**, 63-67.

[12] P. Veerakumar, A. Sangili, S. Manavalan, P. Thanasekaran and K. C. Lin, *Industrial & Engineering Chemistry Research*, 2020, **59**, 6347-6374.

[13] C. G. Liu, Z. N. Yu, D. Neff, A. Zhamu and B. Z. Jang, *Nano Letters*, 2010, **10**, 4863-4868.

[14] L. L. Zhang and X.S. Zhao, *Chemical Society Reviews*, 2009, **38**, 2520–2531.

[15] E. Frackowiak, V. Khomenko, K. Jurewicz, K. Lota and F. J. Beguin, *Power Sources*, 2006, **153**, 413–418.

[16] K. S. Novoselov, A. K. Geim, S. V. Morozov, D. Jiang, Y. Zhang, S. V. Dubonos, I. V. Grigorieva and A. A. Firsov, *Science*, 2004, **306**, 666–669.

[17] A. Balandin, S. Ghosh, W. Bao, I. Calizo, D. Teweldebrhan, F. Miao and C. N. Lau, *Nano Letters*, 2008, **8**, 902–907.

[18] C. Lee, X. Wei, J. W. Kysar and J. Hone, *Science*, 2008, **321**, 385–388.

[19] B. Z. Jang and Z. J. Aruna, *Journal of Material Science*, 2008, **43**, 5092–5101.

[20] S. Park and R. Ruoff, *Nature Nanotechnology*, 2009, **4**, 217–224.

[21] J. Xia, F. Chen, J. Li and N. Tao, *Nature Nanotechnology*, 2009, **4**, 505–509.

[22] Technical System Targets: Onboard Hydrogen Storage for Light-Duty Fuel Cell Vehicles, https://www.energy.gov/, (accessed September 2020).

[23] M. Sadaghiani and M. Mehrpooya, *International Journal of Hydrogen Energy*, 2017, **42**, 6033-6050.

[24] B. Sakintuna, F. Lamaridarkrim and M. Hirscher, *International Journal of Hydrogen Energy*, 2007, **32**, 1121-1140.

[25] J. Vajo, S. Skeith and F. Mertens, *ChemInform*, 2005, 36.

[26] N. Kariya, A. Fukuoka and M. Ichikawa, *Applied Catalysis A: General*, 2002, **233**, 91-102.

[27] S. R. Batten, N. R. Champness, X. M. Chen, J. Garcia-Martinez, S. Kitagawa, L. Ohrstrom, M. O'Keefe, M. P. Suh and J. Reedijk, *Pure and Applied Chemistry*, 2013, **85**, 1715-1724.

[28] A. Ahmed, S. Seth, J. Purewal, A. G. Wong-Foy, M. Veenstra, A. J. Matzger and D. J. Siegel, *Nature Communications*, 2019, **10**, 1568.

[29] Graphene as suitable hydrogen storage substance, https://physicsworld.com, (accessed July 2020).

[30] H. W. Langmi, *Hydrogen Storage in Zeolites and Carbon Materials*, University of Birmingham, 2004.

[31] A. W. C. van den Berg and C. O. Areán, *Chemical Communications*, 2008, **6**, 668-681.

[32] S. Dalai, V. Savithri, P. Shrivastava, S. Param Sivam and P. Sharma, *International Journal of Energy Research*, 2015, **39**, 717-726.

[33] J. Rouquerol, D. Avnir, C. W. Fairbridge, D. H. Everett, J. M. Haynes, N. Pernicone, J. D. F. Ramsay, K. S. W. Sing, K. K. Unger, Pure and Applied Chemistry, 1994, **66**, 1739–1758.

[34] S. Ghosh and A. R. Barron, *Sustainable Energy & Fuels*, 2017, **1**, 806-813.

[35] T. Wang, Y. Zhai, Y. Zhu, C. Li and G. Zeng, *Renewable and Sustainable Energy Reviews*, 2018, **90**, 223-247.

[36] M. Sevilla, A. B. Fuertes, *Carbon*, 2009, **47**, 2281–2289.

[37] L. L. Zhang, X. S. Zhao, *Chemical Society Reviews*, 2009, **38**, 2520–2531.

[38] E. Frackowiak, V. Khomenko, K. Jurewicz, K. Lota, F. J. Beguin, *Power Sources*, 2006, **153**, 413–418.

[39] S. Singhal and A. Shukla, *Journal of Solid State Electrochemistry*, 2020, **24**, 1271-1282.

[40] M. Vadiyar, S. Bhise, S. Patil, S. Kolekar, A. Shelke, N. Deshpande, J. Chang, K. Ghule and A. Ghule, *Chemical Communications*, 2016, **52**, 2557-2560.

[41] Z. Fan, J. Yan, T. Wei, L. Zhi, G. Ning, T. Li , F. Wei, *Advanced Functional Materials*, 2011, **21**, 2366–2375.

[42] V. Fierro, A. Szczurek, C. Zlotea, J. F. Mareche, M. T. Izquierdo, A. Albiniak, M. Latroche, G. Furdin and A. Celzard, *Carbon*, 2010, **48**, 1902.

[43] M. Jorda-Beneyto, F. Suarez-Garcia, D. Lozano-Castello, D. Cazorla-Amoros and A. Linares-Solano, *Carbon*, 2007, **45**, 293.

[44] M. Monteiro de Castro, M. Martinez-Escandell, M. Molina-Sabio and F. Rodriguez-Reinoso, *Carbon*, 2010, **48**, 636.

[45] W. Zhao, V. Fierro, C. Zlotea, E. Aylon, M. T. Izquierdo, M. Latroche and A. Celzard, *International Journal of Hydrogen Energy*, 2011, **36**, 11746.

[46] R. Chetty, S. Kundu, W. Xia, M. Bron, W. Schuhmann, V. Chirila, W. Brandl, T. Reinecke and M. Muhler, *Electrochimica Acta*, 2009, **54**, 4208–4215.

[47] V. Parambhath, R. Nagar and S. Ramaprabhu, *Langmuir*, 2012, **28**, 7826-7833.

[48] Y. Shao, J. Sui, G. Yin, Y. Gao, *Applied Catalysis*, 2008, **79**, 89–99.

[49] R. Prins, *Chemical Reviews*, 2012, **112**, 2714.

[50] R. Juarez-Mosqueda, A. Mavrandonakis, A. Kuc, L. Pettersson and T. Heine, *Frontiers in Chemistry*, 2015, **3**, 1-9.

[51] S. S. Han, H. Jung, D. H. Jung, S. H. Choi, and N. Park, *Physical Review*, 2012, **85**, 155408.

[52] N. Padmanathan, S. Selladurai, K. M. Razeeb, *RSC Advances*, 2105, **5**, 12700–12709.

[53] J. S. Shaikh, R. C. Pawar, R. S. Devan, Y. R. Ma, P. P. Salvi, S. S. Kolekar and P. S. Patil, *Electrochimica Acta*, 2011, **56**, 2127–2134.

[54] A. Hodaei, A. S. Dezfuli and H. R. Naderi, *Journal of Material Science: Materials in Electronics*, 2018, **29**, 14596–14604.

[55] X. Lang, A. Hirata, T. Fujita, M. Chen, *Nature Nanotechnology*, 2011, **6**, 232–236.

[56] R. R. Salunkhe, J. Tang, Y. Kamachi, T. Nakato, J. H. Kim, Y. Yamauchi, *ACS Nano*, 2015, **9**, 6288–6296.

[57] V. Tozzini and V. Pellegrini, *Physical Chemistry Chemical Physics*, 2013, **15**, 80-89.

[58] S. Patchkovskii, J. S. Tse, S. N. Yurchenko, L. Zhechkov, T. Heine and G. Seifer, *Proceedings of the National Academy of Sciences of the United States of America*, 2005, **102**, 10439.

[59] R. Nagar, B. Vinayan, S. Samantaray and S. Ramaprabhu, *Journal of Materials Chemistry A*, 2017, **5**, 22897-22912.

[60] G. Srinivas, Y. Zhu, R. Piner, N. Skipper, M. Ellerby and R. Ruoff, *Carbon*, 2010, **48**, 630–635.

[61] A. G. Klechikov, G. Mercier, P. Merino, S. Blanco, C. Merino and A. V. Talyzin, *Microporous Mesoporous Materials*, 2015, **210**, 46–51.

[62] A. Klechikov, G. Mercier, T. Shari, I. A. Baburin, G. Seifert and A. V. Talyzin, *Chemical Communications*, 2015, **51**, 15280–15283.

[63] G. K. Dimitrakakis, E. Tylianakis and G. E. Froudakis, *Nano Letters*, 2008, **8**, 3166–3170.

[64] S. Yadav, Z. Zhu and C. V. Singh, *International Journal of Hydrogen Energy*, 2014, **39**, 4981–4995.

[65] W. G. Hong, B. H. Kim, S. M. Lee, H. Y. Yu, Y. J. Yun, Y. Jun, J. B. Lee and H. J. Kim, *International Journal of Hydrogen Energy*, 2012, **37**, 7594–7599.

[66] B. P. Vinayan, R. Nagar and S. Ramaprabhu, *Langmuir*, 2012, **28**, 7826–7833.

[67] M. Mohan, V. Sharma, E. Kumar and V. Gayathri, *Energy Storage*, 2019, **1**, 35.

[68] Y. Hao, Y. H. Kim, A. C. Dillon, M. J. Heben, S. B. Zhang, *Physical Review Letters*, 2005, **94**, 15504-15504.

[69] T. Yildirim, J. Iniguez, S. Ciraci, *Physical Review B*, 2005, **72**, 153403-153404.

[70] S. Iijima and T. Ichihashi, *Nature.*, 1993, **363**, 603–605.

[71] S. Iijima, *Nature.*, 1991, **354**, 56–58.

[72] A. C. Dillon, K. M. Jones, T. A. Bekkedahl, C. H. Kiang, D. S. Bethune and M. J. Heben, *Nature.*, 1997, **386**, 377-379.

[73] S. Haukka E. L. Lakomaa and T. Suntola, *Studies in Surface Science and Catalysis*, 1999, **120**, 715-750.

[74] J. van Ommen and G. Bond, *Applied Catalysis*, 1987, **30**, 196-198.

[75] B. Cullity, *Elements of X-ray diffraction*, Addison-Wesley, Reading, 1978.

[76] S. Brunauer, P. H. Emmett and E. Teller, *Journal of the American Chemical Society*, 1938, **60**, 309–319.

[77] G. Halsey, *The Journal of Chemical Physics*, 1948, **16**, 931.

[78] J. Rouquerol, P. Llewellyn and F. Rouquerol, *Studies in Surface Science and Catalysis*, Elsevier, 2007, **160**, 49–56.

[79] K. Kaneko, C. Ishii, M. Ruike and H. Kuwabara, *Carbon*, 1992, **30**, 1075–1088.

[80] A. J. Bard and L. R. Faulkner, *Electrochemical methods and applications*, Wiley-Interscience, New York, 2000.

[81] J. Heinze, *Angewandte Chemie*, 1984, **23**, 831–847.

[82] N. Elgrishi, K. Rountree, J. McCarthy, B. D. Rountree, S. E. Eisenhart, T. Thomas and D. L. Jillian, *Journal of Chemical Education*, 2017, **95**, 197.

[83] S. Singhal and A. Shukla, *Journal of Solid State Electrochemistry*, 2020, **24**, 1271-1282.

[84] P. Kissinger and W. Heineman, *Laboratory techniques in electroanalytical chemistry*, Marcel Dekker, New York, 1996.

[85] A. M. Prokhorov, *Great Soviet Encyclopaedia 3rd edition*, CPSU, Moscow, 1972.

[86] E. Oguz Koroglu, H. Civelek Yoruklu, A. Demir and B. Ozkaya, *Microbial Electrochemical Technology*, 2019, **1**, 565-583.

[87] Y. Sato, K. Yomogida, T. Nanaumi, K. Kobayakawa, Y. Ohsawa and M. Kawai, *Electrochemical and Solid-State Letters*, 1999, **3**, 113.

[88] T. Nanaumi, Y. Ohsawa, K. Kobayakawa and Y. Sato, *Electrochemistry*, 2002, **70**, 681-685.

[89] P. Simon and Y. Gogotsi, *Nature Materials*, 2008, **7**, 845.

[90] Y. Murakami, J. Li and T. Shimoda, *Materials Letters*, 2015, **152**, 121-124.

[91] M. Ho, P. Khiew, D. Isa, T. Tan, W. Chiu and C. Chia, *Nano Letters*, 2014, **9,** 14300-14302.

[92] M. Zheng, R. Li, X. He, X. Dong, P. Ling, N. Zhao, X. Zhang, M. Yu and M. Wu, *Advanced Materials Research*, 2011, **347**, 3370-3374.

[93] J. H. Jang, S. Han, T. Hyeon and S. M. Oh, *Journal of Power Sources*, 2003, **123**, 79.

[94] J. Sieben, E. Morallón and D. Cazorla-Amorós, *Energy*, 2013, **58**, 519-526.

[95] J. J. Jow, H. J. Lee, H. R. Chen, M. S. Wu, T. Y. Wei, *Electrochimica Acta*, 2007, **52**, 2625-2633.

[96] M. Metikoš-Huković, R. Babić, F. Jović and Z. Grubač, *Electrochimica Acta*, 2006, **51**, 1157-1164.

[97] Y. Lee, H. Park, S. Park and I. Song, *Current Applied Physics*, 2012, **12**, 233-237.

[98] Y. Ren, C. Sun, M. Song and L. Wang, *International Journal of Electrochemical Science*, 2016, **11**, 10706-10714.

[99] J. Zhang, D. Shu, T. Zhang, H. Chen, H. Zhao, Y. Wang, Z. Sun, S. Tang, X. Fang and X. Cao, *Journal of Alloys and Compounds*, 2012, **1**, 532.

[100] G. H. Yuan, Z. H. Jiang, A. Aramata and Y. Z. Gao, *Carbon*, 2005, **43**, 2913.

[101] S. Li, K Han, Y. Gao, M. Zhang and Q. Wang, *International Journal of Electrochemical Science*, 2019, **14**,10775-10789.

[102] K. Lee, M. Park and J. Kim, *Colloids and Surfaces A: Physicochemical and Engineering Aspects*, 2017, **533**, 323-329.

[103] Xie, J. Li, Y. Lai, W. Lu, Z. A. Zhang, Y. Liu, L. Zhou and H. Huang, *Electrochemical Communications*, 2011, **13**, 657.

[104] X. Zhao, C. Johnston and P. S. Grant, *Journal of Materials Chemistry*, 2009, **19**, 8755.

[105] S. Park, C. Raj, R. Manikandan, B. Kim and K. Yu, *Bulletin of the Korean Chemical Society*, 2020, **41**, 856-863.

[106] A. C. Rodrigues, E. da Silva, A. Oliveira, J. Matsushima, A. Cuña, J. Marcuzzo, E. Gonçalves and M. Baldan, *Materials Today Communications*, 2019, **21**, 1005-1053.

[107] H. S. Jadhav, A. Roy, W.-J. Chung and J. G. Seo, *Electrochimica Acta*, 2017, **246**, 941.

[108] X. Jiang, G. Shi, G. Wang, P. Mishra, J. Du and Y. Zhang, *Ionics*, 2020, **26**, 4039-4051.

[109] H. Lee, Y. K. Park, S. J. Kim, B. J. Kim, K. H. An, B. H. Kim and S. C. Jung, *Journal of Nanoscience and Nanotechnology*, 2016, **16**, 4483–4486.

[110] Q. Chen, J. Li and Y. Li, *Journal of Physics D: Applied Physics*, 2015, **48**, 4240-4245.

[111] H. Lee, S. J. Kim, K. H. An, J. S. Kim, B. H. Kim and S. C. Jung, *Advanced Materials Letters*, 2016, **7**, 98–103.

[112] H. Lee, W. Lee, Y. Park, S. Ki, B. Kim and S. Jung, *Nanomaterials*, 2018, **8**, 190.

[113] I. Oh, M. Kim and J. Kim, *Energy*, 2015, **86**, 292-299.

[114] L. Wang, H. Ji, S. Wang, L. Kong, X. Jiang and G. Yang, *Nanoscale*, 2013, **5**, 3793-3799.

[115] N. L. Wu, *Materials Chemistry and Physics*, 2002, **6**, 75.

[116] S. Ki, K. Jeon, Y. Park, H. Park, S. Jeong, H. Lee and S. Jung, *Journal of Environmental Management*, 2017, **203**, 880-887.

[117] S. Chang, Z. Zainal, K. Tan, N. Yusof, W. Yusoff and S. Prabaharan, *Current Applied Physics*, 2012, **12**, 1421-1428.

[118] H. Lee, I. Park, Y. Park, K. An, B. Kim and S. Jung, *Nanomaterials*, 2019, **10**, 61.

[119] E. Atibu, N. Devarajan, A. Laffite, G. Giuliani, J. Salumu, R. Muteb, C. Mulaji, J. Otamonga, V. Elongo, P. Mpiana and J. Poté, *Geochemistry*, 2016, **76**, 353-362.

[120] B. Tan and J. M. Lee, *Journal of Materials Chemistry A*, 2013, **1**, 14814-14843.

[121] Y. Zhu, X. Lv, L. Zhang, X. Guo, D. Liu, J. Chen and J. Ji, *Electrochimica Acta*, 2016, **215**, 247-252.

[122] Z. Hu, K. Ma, W. Tian, F. Wang, H. Zhang, J. He, K. Deng, Y.X. Zhang, H. Yue and J. Ji, *Applied Surface Science*, 2020, **508**, 14477-14484.

[123] L. L. Zhang, R. Zhou and X. Zhao, *Journal of Materials Chemistry*, 2010, **20**, 5983-5992.

[124] X. Meng, L. Lu and C. Sun, *ACS Applied Materials & Interfaces*, 2018, **10**, 16474-16481.

[125] D. Wu, H. Han, X. Hong, S. Tao, S. Xu, B. Qian, L. Wang, X. Chen and P. Chu, *Journal of Alloys and Compounds*, 2020, **846**, 155720.

[126] C. Xiao, X. Zhang, T.C. Mendes, G.P. Knowles, A.L. Chaffee and D. MacFarlane, *Journal of Physical Chemistry C*, 2016, **120**, 23976-23983.

[127] X. Yang, C. Xiang, Y. Zou, J. Liang, H. Zhang, E. Yan, F. Xu, X. Hu, Q. Cheng and L. Sun, *Journal of Materials Science & Technology*, 2020, **55**, 223-230.

[128] S. Sarwar, Z. Liu, J. Li, Y. Wang, R. Wang and X. Zhang, *Journal of Alloys and Compounds*, 2020, **846**, 155886.

[129] S. J. Park and S. Y. Lee, *International Journal of Hydrogen Energy*, 2010, **35**, 13048–13054.

[130] A. D. Lueking and R. T. Yang, *Applied Catalysis A: General*, 2004, **265**, 259–268.

[131] S. C. Mu, H. L. Tang, S. H. Qian, P. Mu and R. Z. Yuan, *Carbon*, 2006, **44**, 762–767.

[132] M. Aboud, Z. Al Othman, M. Habila, C. Zlotea, M. Latroche and F. Cuevas, *Energies*, 2015, **8**, 3578-3590.

[133] N. Bader and A. Ouederni, *Journal of Energy Storage*, 2017, **13**, 268-276.

[134] W. Henry, *Philosophical Transactions of the Royal Society of London*, 1803, **93**, 29-274.

[135] W. Zhao, V. Fierro, C. Zlotea, C. Chevalier-César, M. T. Izquierdo, M. Latroche and A. Celzard, *International Journal of Hydrogen Energy*, 2012, **27**, 5072–5080.

[136] C. Zlotea, F. Cuevas, V. P. Boncour, E. Leroy, P. Dibandjo, R. Gadiou, C. V. Guterl and M. Latroche, *Journal of the American Chemical Society*, 2010, **132**, 7720–7729.

[137] Y. Li, R. Yang, C. Liu and Z. Wang, *Industrial & Engineering Chemistry Research*, 2007, **46**, 8277-8281.

[138] M. Zieliński, R. Wojcieszak, S. Monteverdi, M. Mercy and M. Bettahar, *Catalysis Communications*, 2005, **6**, 777-783.

[139] J. Amiel, P. Delhaes, F. Beguin and R. Setton, *Materials Science and Engineering*, 1977, **31**, 243.

[140] A. Legrand, L. Facchini, D. Bonnin, J. Bouat, M. Quinton and F. Beguin, *Synthetic Metals*, 1985, **12**, 175-180.

[141] D. Saha, C. Contescu and N. Gallego, *Langmuir*, 2012, **28**, 5669-5677.

[142] A. Minoda, S. Oshima, H. Iki and E. Akiba, *Journal of Alloys and Compounds*, 2014, **606**, 112-116.

[143] H. Zhang, V. Bhat, P. Feng, C. Contescu and N. Gallego, *Carbon*, 2012, **50**, 5278-5285.

[144] G. Kim, S. Jhi, S. Lim and N. Park, *Applied Physics Letters*, 2009, **94**, 173102.

[145] M. López, I. Cabria and J. Alonso, *The Journal of Physical Chemistry C*, 2014, **118**, 5081-5090.

[146] J. Li, T. Furuta, H. Goto, T. Ohashi, Y. Fujiwara and S. Yip, *The Journal of Chemical Physics*, 2003, **119**, 2376-2385.

[147] V. Parambhath, R. Nagar and S. Ramaprabhu, *Langmuir*, 2012, **28**, 7826-7833.

[148] D. P. and S. Ramaprabhu, *Physical Chemistry Chemical Physics*, 2014, **16**, 26725-26729.

[149] H. Jung, K. Park, M. Gueye, S. So and C. Park, *International Journal of Hydrogen Energy*, 2016, **41**, 5019-5027.

[150] L. Yuan, Y. Chen, L. Kang, C. Zhang, D. Wang, C. Wang, M. Zhang and X. Wu, *Applied Surface Science*, 2017, **399**, 463-468.

[151] F. Yasareh, A. Kazempour and R. Behjatmanesh-Ardakani, *Journal of Molecular Modelling*, 2020, **26**, 96-104.

[152] U. Sahaym and M. Norton, *Journal of Materials Science*, 2008, **43**, 5395-5429.

[153] J. Wang, Y. Chen, L. Yuan, M. Zhang and C. Zhang, *Molecules*, 2019, **24**, 2382.

[154] L. Wang, K. Lee, Y. Sun, M. Lucking, Z. Chen, J. Zhao and S. Zhang, *ACS Nano*, 2009, **3**, 2995-3000.

[155] D. Elias, R. Nair, T. Mohiuddin, S. Morozov, P. Blake, M. Halsall, A. Ferrari, D. Boukhvalov, M. Katsnelson, A. Geim and K. Novoselov, *Science*, 2009, **323**, 610-613.

[156] S. Chu, L. Hu, X. Hu, M. Yang and J. Deng, *International Journal of Hydrogen Energy*, 2011, **36**, 12324-12328.

[157] T. Mashoff, D. Convertino, V. Miseikis, C. Coletti, V. Piazza, V. Tozzini, F. Beltram and S. Heun, *Applied Physics Letters*, 2015, **106**, 83901.

[158] C. Cavallari, S. Rols, H. Fischer, M. Brunelli, M. Gaboardi, G. Magnani, M. Riccò and D. Pontiroli, *International Journal of Hydrogen Energy*, 2019, **44**, 30999-31007.

[159] J. Gu, X. Zhang, L. Fu and A. Pang, *International Journal of Hydrogen Energy*, 2019, **44**, 6036-6044.

[160] L. Antipina, P. Avramov, S. Sakai, H. Naramoto, M. Ohtomo, S. Entani, Y. Matsumoto and P. Sorokin, *Physical Review B*, 2012, **86**, 85435.

[161] S. Lee and S. Jhi, *Carbon*, 2015, **81**, 418-425.

[162] R. Heimann, S. Evsvukov and Y. Koga, *Carbon*, 1997, **35**, 1654-1658.

[163] A. N. Enyashin and A. L. Ivanovskii, *Physica Status Solidi B*, 2011, **248**, 1879–1883.

[164] Y. Ye, C. C. Ahn, C. Witham, and B. Fultz, *Applied Physics Letters*, 1999, **74**, 2307.

[165] W. Deng, X. Xu and W. Goddard, *Physical Review Letters*, 2004, **92**, 166103.

[166] F. E. Pinkerton, *Journal of Physical Chemistry B*, 2000, **10**, 9460.

[167] M. Hirscher, M. Becher, M. Haluska, U. Dettlaff-Weglikowska, A. Quintel, G.S. Duesberg, Y.-M. Choi, P. Downes, M. Hulman, S. Roth, I. Stepanek and P. Bernier, *Applied Physics A: Materials Science and Processing*, 2001, **72**, 129.

[168] E. Rangel, J. Ramirez-de-Arellano and L. Magana, *Physica Status Solidi B*, 2010, **248**, 1420-1424.

[169] Y. Wang, A. Li, K. Wang, C. Guan, W. Deng, C. Li and X. Wang, *Journal of Materials Chemistry*, 2010, **20**, 6490.

[170] M. Mehrabi, P. Parvin, A. Reyhani and S. Mortazavi, *International Journal of Hydrogen Energy*, 2018, **43**, 12211-12221.

[171] K. Chandrakumar and S. Ghosh, *Nano Letters*, 2008, **8**, 13-19.

[172] Y. Zhao, Y. H. Kim, A. C. Dillon, J. M. Heben and S. B. Zhang, *Physics Review Letters*, 2005, **94**, 155504.

[173] T. Yildirim, J. Íñiguez and S. Ciraci, *Physical Review B*, 2005, **72**, 153403.

[174] D. Saha and S. Deng, *Langmuir*, 2011, **27**, 6780-6786.

[175] K. Srinivasu and S. Ghosh, *The Journal of Physical Chemistry C*, 2012, **116**, 25184-25189.

[176] B. Palpant, N. M. Sanekata, K. Miyajima, S. Nagao, K. Judai, D. M. Rayner, B. Simard, P. A. Hackett, A. Nakajima and K. J. Kaya, *Chemical Physics*, 2001, **114**, 8459.